Cell-Surface RNA Associates with Heparan Sulfate and RNA-Binding Proteins to Modulate Receptor-Ligand Interactions

Zeshi Li [1, 2, 3, §],*, Bhagyashree S. Joshi [2, §], Ruud H. Wijdeven [4, 5], Irene Santos-Barriopedro [6], Milad Shademan [1], Eric Bos [7], Marvin Tanenbaum [2, 8], Geert-Jan Boons [9, 10], Thomas Sharp [11], Michiel Vermeulen[6, 12], Vered Raz [1, *] & Chirlmin Joo [1, 13, *]

[1] Human Genetics department, Leiden University Medical Centre, 2333ZC Leiden, The Netherlands
[2] Department of BioNanoScience, Kavli Institute of Nanoscience Delft, Delft University of Technology, 2629 HZ, Delft, The Netherlands
[3] Department of Chemical Biology & Drug Discovery, Utrecht Institute for Pharmaceutical Sciences, Utrecht University, 3584 CG Utrecht, The Netherlands
[4] Department of Cell and Chemical Biology, Oncode Institute, Leiden University Medical Center, 2333 ZA Leiden, Zuid-Holland, the Netherlands
[5] Department of Functional Genomics, Center for Neurogenomics and Cognitive Research (CNCR), Vrije Universiteit Medical Center, 1007 MB Amsterdam, Noord-Holland, the Netherlands
[6] Department of Molecular Biology, Faculty of Science, Radboud Institute for Molecular Life Sciences, Oncode Institute, Radboud University Nijmegen, Nijmegen, The Netherlands
[7] Department of Cell and Chemical Biology, Leiden University Medical Center, Leiden 2300 RC, The Netherlands
[8] Oncode Institute, Hubrecht Institute-KNAW and University Medical Center Utrecht, Utrecht, the Netherlands.
[9] Department of Chemical Biology and Drug Discovery, Utrecht Institute for Pharmaceutical Sciences, Utrecht University, Utrecht, The Netherlands.
[10] Bijvoet Center for Biomolecular Research, Utrecht University, Utrecht, The Netherlands
[11] School of Biochemistry, University of Bristol, Bristol BS8 1TD, U.K.
[12] Division of Molecular Genetics, The Netherlands Cancer Institute, Amsterdam, The Netherlands
[13] Department of Physics, Ewha Womans University, Seoul 03760, Republic of Korea

§: equal contribution
*: corresponding authorship

Abstract

Recent discoveries have shown the presence of RNA molecules on the cell surface, defying the traditional view that RNA only functions intracellularly. However, it is not well understood how cell-surface RNA (csRNA) is stably present on the plasma membrane and what functions it performs on the cell surface. By exploiting the RNA-sensing ability of TLR7 as a specific recombinant probe to detect csRNA and coupling it with a genome-wide CRISPR-Cas9- knockout screening to identify genes essential for csRNA presentation on cells, we identified heparan sulfate (HS) as a crucial factor for RNA presentation on cells. Using the TLR7 binding probe, cell surface proximity labelling revealed that csRNA associates mechanistically with a plethora of RNA-binding proteins, and these interactions are crucial for csRNA presentation. Moreover, csRNA modulates receptor-ligand interactions between poliovirus receptor (PVR) and killer cell immunoglobulin-like receptor 2DL5 (KIR2DL5) by acting as a co-binder, recruiting the latter to cell surface. We provide a mechanistic understanding of csRNA presentation and unveil a new layer of complexity in the csRNA-dictated regulation of cell surface receptor-ligand interactions.

Introduction

Ribonucleic acid (RNA) performs many critical cellular functions in both prokaryote and eukaryote cells. Although the localization of RNA was considered primarily intracellular in mammalian cells, emerging studies have indicated that RNA can be displayed on the cell surface. A previous study found that bacterial genome-encoded RNA can be anchored on their cell surface via binding to a protein.[1] Very recent studies have shown the presence of RNA on the extracellular part of mammalian cell plasma membranes.[2-5] These cell-surface-associated RNAs (csRNAs) include fragments of messenger and long non-coding RNAs and putative glycosylated small RNAs. There are indications that csRNAs can participate in molecular recognition, thereby modulating cell-cell interactions. A recent study has shown csRNA mediated neutrophil recruitment by interacting with P-selectin on the endothelial cells.[6] Despite the aforementioned studies, mechanistic understanding as to how RNAs are stably presented on the mammalian cell surface remains limited. It is also unclear if csRNA may exhibit other modes of function besides presenting glycan moieties to interacting cells.[2,6]

As most RNA molecules are associated with RNA-binding proteins (RBPs), it can be speculated that csRNA is similarly associated with RBPs, providing a mechanism for cell surface anchoring. In line with this hypothesis, both earlier and recent studies have demonstrated RBPs, previously thought to be localized only intracellularly, are also present on the plasma membrane.[7-10] Thus, the potential binding partners are indeed available for and in proximity to RNA on the cell surface. However, these RBPs are generally soluble proteins that do not possess a transmembrane domain and are therefore unlikely to be directly anchored on the lipid bilayer like many cell-surface glycoproteins. For example, a classical nuclear RBP, U5 SNRNP200, has been evaluated as an acute myeloid lymphoma-associated cell surface antigen for immunotherapy.[9, 10] This RBP was shown to be associated with the Fcγ receptor IIIA. A more recent study revealed that a plethora of RBPs can localize to the cell surface, as possible carriers of csRNA.[11] However, it is largely unknown how csRNA and RBPs become stably presented on the plasma membrane, and if so, whether they are associated with each other.

Animal cells employ highly negatively charged linear carbohydrate polymers, such as glycosaminoglycans, as a scaffold to enrich soluble proteins and organize membrane bound proteins on the plasma membrane.[12] Heparan sulfate (HS) is an important class of glycosaminoglycans ubiquitously found on plasma membrane and in extracellular matrix (ECM).[13] Portions of HS are heavily sulfated, and these sulfated domains serve as docking sites for a broad array of proteins, including growth factors, morphogens, amyloid proteins, lipoproteins, cytokines, and chemokines, as well as many microbial proteins. HS is characterized by having an extension of repeating disaccharide units, glucosamine-α1,4-glucuronic acid (GlcN-GlcA) or glucosamine-α1,4-iduronic acid (GlcN-IdoA). An HS chain can contain over a hundred monosaccharide units. Glycan modifications such as N- and O-sulfation introduce negative charges to portions of the HS chain and are known to be crucial for the biological functions of HS. The pattern of N- and O-

sulfation, also known as the sulfation code, critically determines what proteins interact with HS. These features make HS among a main directors of cell surface interactions.[14]

Here, we demonstrate that heparan sulfate (HS) is a scaffold for the presentation of RNAs and RBPs on the cell surface. The key to these findings was the use of toll-like receptor 7 (TLR7) as a probe for csRNA. We established that the recombinant TLR7-Fc fusion protein can be used to detect and capture RNA on the surface of living cells. This enabled us to perform a genome-wide screening to identify genes affecting csRNA localization, which revealed heparan sulfate biosynthetic enzymes as essential factors. The same probe also allowed for the identification of csRNA-proximal proteome, which includes canonical and non-canonical RBPs. Several identified RBPs were validated to localize on the cell surface using immunofluorescence microscopy. Altogether, our data reveals how csRNA is anchored to the plasma membrane: RNA and RBPs form RNP complexes, and these complexes are deposited on the HS chain to ensure stable presentation. We further demonstrated csRNA could recruit killer cell immunoglobulin-like receptor 2DL5 (KIR2DL5) on cell surface, which suggests csRNA may modulate the interaction between KIR2DL5 on an immune cell and PVR on a target cell.

Results

Establishment of TLR7-Fc as a probe for csRNA

The sequence of RNA molecules on the plasma membrane likely varies between different cells, and RNA molecules present at low copy numbers may elude detection.[15] The state-of-the-art csRNA labeling approaches either require fixation or rupturing of the plasma membrane[3, 15] and are therefore not compatible with live cells. To overcome this, we reasoned that the use of an RNA-recognizing probe with low sequence specificity, rather than a hybridizing probe which requires prior knowledge of csRNA sequence, should boost the chance for csRNA detection, and yield strong signals. We, therefore, exploited nature's RNA-sensing machinery: toll-like receptor 7 (TLR7),[16] an endosome-localized, pattern recognition receptor in select immune cells to sense foreign single-stranded RNA molecules. TLR7 requires two consecutive uridine moieties for strong binding, but requires only few other sequence features for RNA binding.[17] We used the ectodomain of TLR7 (Ala27-Asn839) fused to the human Fc tag (denoted hereafter TLR7-Fc). The former is expected to recognize csRNA on intact (live) cells, and the latter will allow for the detection by a secondary antibody for different downstream applications.

We employed confocal microscopy to examine the efficiency of TLR7-Fc detecting csRNA. TLR7-Fc is applied onto intact, fixed cells without cell permeabilization, followed by washing and the addition of a fluorophore-conjugated, anti-human IgG secondary antibody. To check for localization of TLR7-Fc staining, we labeled the cell surface with biotin-conjugated wheat germ agglutinin (WGA),[18] a lectin that recognizes N-acetylneuraminic acid and N-acetylglucosamine residues present in cell surface glycans, and the biotin moieties were detected by fluorescent streptavidin. We observed that bright puncta given rise to by TLR7-Fc probe in complex with the

fluorescent secondary antibody align with the rims of HeLa, U2OS, and Mel526 cells (**Figure 1a** and **Supplementary Figure 1a** and **b**). This is akin to many cell surface proteins, which manifest in clusters.[19, 20] WGA signal remained confined to the cell surface. csRNA signal was absent in controls devoid of TLR7-Fc, but including only the secondary antibody (**Supplementary Figure 1c**). Further, a treatment with RNaseA/T1 cocktail in fixed, non-permeabilized cells, severely disrupted the TLR7 signal (**Figure 1a**), while DNase treatment did not (**Supplementary Figure 1d**), validating the RNA specificity of TLR7 binding. Moreover, the presence of excess exogenously added single-stranded RNA in solution competitively inhibited the TLR7 signal, further supporting the specificity of TLR7 to probe RNA (**Figure 1a**). Live-cell staining with TLR7 showed the same puncta pattern, indicating that the clustering of our probe on the cell surface is unlikely to be caused by cell fixation (**Supplementary Figure 1e**).[21-23] Interestingly, the monoclonal antibody J2, previously used for intracellular detection of endogenous dsRNA[24] and viral dsRNA,[25] as well as for cell-surface detection glycoRNA,[2] did not give detectable signals on HeLa or U2OS cell surface (**Supplementary Figure 1f**).

We further used our TLR7-Fc probe to quantify csRNA and its sensitivity to RNase treatment with flow cytometry. Corroborating the fluorescence imaging results, when live cells were pre-treated with RNase A, the signal intensity given rise by TLR7-Fc in complex with the fluorescent secondary antibody dropped dramatically close to the background. (**Figure 1b** and **Supplementary Figure 2a**). To further confirm that TLR7-Fc binds to RNA on the cell surface, the prior csRNA-depleted cells by RNase were incubated with exogenous, purified total cellular RNA. We found that TLR7 binding could be partly restored by exogenous RNA in a concentration-dependent manner (**Figure 1c** and **Supplementary Figure 2b**).

To further validate that TLR7 binds to RNA on the cell surface, we performed in-situ RNA-protein crosslinking with UVC (254 nm) after TLR7-Fc probe addition, followed by RNA precipitation and RNA 3'-end labeling (**Figure 1d**). Upon UVC irradiation, csRNA is expected to be covalently bound to the TLR7-Fc probe and can be co-precipitated with the probe using protein A-functionalized magnetic beads. The precipitated RNA was then labeled at the 3'-end with biotin-cytidine using RNA ligase 1. This was followed by SDS-PAGE and Western blot for biotin. As a negative control, cells were UVC irradiated before TLR7-Fc incubation and subjected to the same procedure. UVC-crosslinked biotinylated csRNA is expected to remain bound to TLR7 throughout the entire procedure, whereas the csRNA not crosslinked to TLR7 will dissociate upon denaturation, and therefore will not remain on the blotting membrane.[26] We observed a strong chemiluminescent signal above TLR7-Fc molecular weight for crosslinked csRNA-TLR7 (**Figure 1e**), but not for non-crosslinked TLR7 probe. These results demonstrate TLR7 probe binds to RNA on the cell surface. Moreover, this demonstrates that TRL7 can be used to capture and isolate csRNA. Next, to understand the cell surface organization of csRNA at high resolution, we employed electron microscopy (EM), leveraging the TLR7-Fc probe and Protein-A-gold (10 nm)

as a secondary probe (**Supplementary Figure 3a** and **b**) where we observed multiple csRNA signals along the cellular periphery, confirming the findings with fluorescent microscopy.

Genome-wide screening identified cellular factors required for csRNA presentation

Previous studies have only postulated that csRNA can be presented on the plasma membrane, yet a detailed mechanistic understanding of this process is lacking. With TLR7-Fc as a general csRNA probe in hand, we next sought to uncover the molecular underpinnings of csRNA presentation. We performed a pooled genome-wide, CRISPR-Cas9-mediated knockout (KO) screening[27] to identify essential cellular factors for csRNA stable presentation. TLR7-Fc in complex with a fluorescent secondary antibody was used to enrich the csRNA^{low} population with fluorescence-assisted cell sorting (FACS). Such FACS-based enrichment was performed twice. The enriched cells together with the non-enriched input cells were subjected to deep sequencing to identify the guide RNAs of CRISPR-Cas9 giving rise to the csRNA^{low} phenotype. (**Figure 2a**, see **Supplementary Figure 4** for gating strategies).

Data analysis revealed that enzymes involved in heparan sulfate (HS) biosynthesis[28] were among the highest-scoring hits, suggesting HS is a pivotal molecular factor for the stable cell-surface display of RNAs (**Figure 2b**, full list of hits in **Supplementary Table 1**). Our hits include enzymes for the core tetrasaccharide synthesis (XYLT2, B4GALT7, B3GALT6, and B3GAT3), glycan chain polymerizing enzymes (EXT1, EXT2, and EXTL3), as well as glycan chain modifying enzymes such as sulfotransferases (NDST1, HS2ST1, and HS6ST1) and a xylose kinase (FAM20B) (**Figure 2c**). These hits suggest the stable presentation of csRNA requires a fully extended HS chain and appropriate N- and O-sulfation pattern.

Apart from the HS-related glycosyltransferases and glycan-modifying enzymes, we also identified regulators in HS biosynthesis. For example, UGDH oxidizes uridine diphosophate linked glucose (UDP-Glc) to UDP-GlcA, a glycosyl donor for HS polymerization; SLC35B2 is a Golgi membrane transporter of the sulfo-donor, adenosine 3'-phospho-5'-phosphosulfate;[29] SLC10A7 is crucial for cellular calcium regulation and was implicated in HS biosynthesis;[30] and C3orf58 has been recently shown to regulate HS biosynthesis.[31] The genes related to the N-glycan biosynthetic pathway were not among the candidates, suggesting the csRNA detected by TLR7 is independent from glycoRNA, and it does not require N-glycosylation to access plasma membrane.

Validation of HS's essentiality for stable csRNA presentation

Next, our attention was focused on validating that HS is necessary for a display of the csRNA detected by the TLR7-Fc probe. csRNA location closely correlated with the heparan sulfate staining on the cell surface showing their tight proximity (**Figure 2d**). We then generated HS-deficient mutant cells lacking either the elongation enzyme EXT2 or sulfotransferase HS6ST1 via CRISPR-Cas9 mediated KO, each with two high-scoring guide RNAs, and used flow cytometry to quantify TLR7-Fc binding. Both guide RNAs for EXT2 resulted in an almost complete loss of TLR7

binding. The anti-HS IgM (10E4 epitope)[32] confirmed the absence of the HS chain. One guide RNA for HS6ST1 led to a similar phenotype as did EXT2 KO, whereas the other guide RNA reduced TLR7 binding down to approximately 30% of the wild type but did not decrease anti-HS IgM binding (**Figure 2e**). In consistency with the flow cytometry experiments, confocal microscopy also showed a dramatic reduction in csRNA signal around the cell rim after knocking out EXT2, HS6ST1, EXTL3, and C3orf58 (**Supplementary Figure 5a**). The loss of TLR7 binding to the cell rim was also observed in Chinese hamster ovary (CHO) cell mutants (pgsD-677 and pgsE-606) deficient in HS biosynthesis. The wildtype CHO cell showed a similar punctate pattern as did Mel526, although more prevalent (**Supplementary Figure 5b**). Along with the data in **Supplementary Figure 1a** we show that HS supports csRNA stable presentation in other cell lines than Mel526 and is a multispecies phenomenon.

To further validate the genetic screen results, we selected two HS-deficient mutant cells. Cells were first treated with RNase A, and then with exogenous total RNA at varying concentrations (**Supplementary Figure 5c**). The treated cells were then incubated with TLR7-Fc followed by a fluorescent secondary antibody. The TLR7 binding remained close to the background throughout all experimental groups regardless of the RNA concentrations. These results demonstrate that cells lacking an extended HS chain or an appropriate sulfation pattern become refractory to exogenous RNA incubation and can no longer rescue TLR7 binding, suggesting that csRNA presentation requires intact HS. Hereafter, we refer the csRNA detected by the TLR7-Fc probe as heparan sulfate-associated RNA (HepRNA).

RNA-binding proteins on the cell surface

Both RNA and HS are highly negatively charged biopolymers. We next asked how these two macromolecules are interlinked. We were struck by the observation that upon proteolytic detachment of adherent cells by TryPLE before flow cytometry, TLR7-Fc no longer detectably bound to the cell surface (**Supplementary Figure 6a**), while non-tryptic detachment methods such as EDTA, or StemPro Accutase allowed for HepRNA detection by TLR7-Fc. The observation led us to hypothesize that HepRNA may require an additional factor, such as proteins, to be presented on the cell surface HS (**Supplementary Figure 6b**). We, therefore, applied a peroxidase-mediated labeling approach to identify the HepRNA-proximal proteome using TLR7-Fc. Peroxidase-mediated proximity labeling on cell surface has a labeling range of 200-300 nm,[33] and was previously used to identify the composition of membrane protein clusters. To identify proteins proximal to HepRNA, we pre-complexed TLR7-Fc with horse radish peroxidase (HRP)-conjugated protein A, which was then incubated with wild-type and RNase-pretreated Mel526 cells (**Figure 3a**). RNase treatment is expected to digest unprotected regions of HepRNA into smaller fragments, whereas the portions proximal to or bound by a protein are shielded from digestion, an effect commonly exploited to study proteins' footprint on an RNA.[26] As an isotype control, human IgG was used instead of TLR7-Fc. HRP proximal to csRNA catalyzes the formation of short-lived biotin-

phenol (BP) radical in the presence of hydrogen peroxide, and the radical readily attaches to proteins surrounding the HRP catalytic center. Biotinylation of proteins on the cell surface was confirmed by fluorescence imaging Western blotting (**Supplementary Figure 6c** and **d**). Following proximity labeling and non-denaturing cell lysis, biotinylated cell-surface proteins were enriched with streptavidin-functionalized agarose resin. Bound proteins were then on-bead digested with trypsin and subjected to LC-MS/MS and label-free quantitative proteomics analysis.

By comparing the TLR7-proximal proteome of non-treated cells with the IgG isotype control, which we assume only gives background, we identified 266 proteins as significantly enriched hits (full list of hits in **Supplementary Table 2**). Of the significantly e nriched hits, 148 of them carry the gene ontology (GO) term 'cell surface' (GO:0009986) or 'plasma membrane' (GO:0005886), suggesting HepRNA may be spatially close to these proteins. In the RNase-treated cell dataset (**Figure 3b,** full list of hits in **Supplementary Table 3**), these cell surface-localized hits became largely absent, which indicates the partially digested RNA bound by the TLR7 probe complex were no longer proximal to the (glyco)proteins. Interestingly, we also identified a considerable set of 117 proteins that remained consistently enriched in RNase-treated and non-treated cell samples. Among these proteins, 33 carried the GO term 'RNA binding' (GO:0003723), which include classical RNA-binding proteins such as hnRNPA1, hnRNPA2B1, and the lupus La protein (also known as Sjogren syndrome antigen type B), as well as reported non-canonical RNA binding proteins that do not possess a classical RNA-binding domain, many of which are metabolic enzymes or chaperones with moonlighting RNA-binding functions, such as ENO1[34] and CALR.[35] The results suggest the possible presence of these RNA-binding proteins on the cell surface, despite most of them being classically viewed as soluble intracellular proteins.

RNA-binding proteins as anchor points between csRNA and HS

Given the RBP-heparin interactions as observed in previous studies, we postulate that RBP may function to non-covalently connect HepRNA with HS, providing an anchor point for stable RNA presentation on HS. We first selected representative RBPs to validate their presence on the cell surface. These include canonical RBPs that contain RNA-binding domains, such as La protein and heterogeneous nuclear ribonucleoprotein A1 (hnRNPA1), as well as non-canonical RBPs that do not possess a specific RNA-binding domain, such as enolase 1 (ENO1) and proliferation-associated protein 2G4 (PA2G4). La protein staining showed distinct bright punctae which colocalized with TLR7-Fc on wildtype Mel526 cell surface with immunofluorescence via confocal microscopy (**Figure 3c**), and these punctae were largely depleted upon extracellular RNase treatment (**Supplementary Figure 6e**), suggesting the RBP needs to complex with HepRNA to be stably presented on cell surface. The HS-deficient mutant (EXT2 KO) incubated with the same anti-La protein antibody, did not show the punctae (**Figure 3d**). In wildtype Mel526 cells, La protein also colocalized with HS (**Figure 3e**), which was stained with 10E4 monoclonal antibody. Similar results were obtained for hnRNPA1, ENO1, and PA2G4 using the corresponding primary

antibodies, and their staining on the cell surface requires the cell to be competent in HS biosynthesis (**Figure 3f**). Taken together, these results indicate HepRNA, RBP, and HS are in proximity, and that the presence of RBPs on the cell surface requires intact HS.

HepRNA modulates receptor-ligand interaction on cell surface

The concentration of proximal binding proteins and HepRNA in the same domains on the cell surface and the requirement of HepRNA to select protein interaction with the cell surface motivated us to explore the possibility that ligands or receptors from other cells may engage with the HepRNA for their function. Our HepRNA-proximal datasets harbor many membrane glycoproteins which were no longer enriched in response to RNase treatment (**Figure 4a,** full list of hits in **Supplementary Table 4**). We asked if the functions of these RNase-responsive glycoproteins could be modulated by HepRNA. To choose an appropriate hit from the dataset, we have set our selection criteria: 1) the hit has higher value in log2FoldChange than the TLR7-Fc probe (indicated by a red dashed line), implicating HepRNA proximity; 2) the hit is documented in RBP2GO database,[36] indicating the likelihood for RNA interaction.

In our data set (**Figure 4a**), the glycoprotein poliovirus receptor (PVR, or CD155) was enriched by approximately 28 folds, suggesting it is spatially close to HepRNA. Interestingly, in a previous study, the mobility of PVR from cell lysates through a sucrose density gradient dramatically changed upon RNase treatment.[37] Among our HepRNA-proximal hits with log2FoldChange values larger than TLR7, PVR exhibited the largest RNase-responsive mobility shift. PVR was thus selected for further investigation. PVR overexpresses in different cancers and can bind to T cell immunoreceptor with immunoglobulin and ITIM domain (TIGIT),[38] CD96,[39] and Killer cell immunoglobulin-like receptor 2DL5 (KIR2DL5),[40] all of which are inhibitory receptors able to suppress the killing by T cells or NK cells. PVR also interacts with an activating receptor, CD226.[41] The engagement of PVR with these proteins forms immune checkpoints, and they are thus new promising targets for cancer immunotherapy. We have envisioned the possible modes of action of HepRNA on PVR recognition (**Figure 4b**): 1) HepRNA may sterically hinder the binding; 2) HepRNA may facilitate the binding of specific proteins to PVR by functioning as a co-receptor, or by priming PVR for optimal recognition; and finally, 3) HepRNA may be just a bystander, and has no effect on binding.

We used flow cytometry to assess the RNase responsiveness of PVR engagement by the soluble, Fc-tagged version ectodomains derived from the four proteins. We compared their binding to the cell surface with and without RNase pre-treatment (**Figure 4c**). TIGIT and CD226 exhibited little change in response to RNase treatment, indicating that HepRNA does not modulate their recognition. CD96 did not detectably bind to either cell surface in our experimental settings, suggesting additional factors may be required. KIR2DL5 did show a dramatic reduction in fluorescent signals on the cell surface when the live cells were pretreated with RNase. In line with the genetic screening data, the EXT2 KO mutant cells also exhibited a strong reduction in KIR2DL5

binding, but not for CD226 or TIGIT (**Figure 4d**). Neither the RNase treatment nor EXT2 KO negatively affected cell-surface PVR levels (**Supplementary Figure 7a** and **b**), indicating that the decrease in KIR2DL5 binding was due to HepRNA removal, rather than an effect on PVR expression. Exogenous RNA added to prior HepRNA-depleted cells restored partly KIR2DL5 binding (**Supplementary Figure 7c**), demonstrating the dependency of KIR2DL5 recruitment on HepRNA. To confirm the binding of KIR2DL5 proteins to the cell surface is at least partly dependent on PVR, we generated PVR knockout cells using CRISRP-Cas9. Upon treatment with extracellular RNase, the residual KIR2DL5 binding was significantly lower in PVR KO cells than in the wild type (**Supplementary Figure 7d**). This indicated that KIR2DL5-PVR interaction accounted for a portion of fluorescence signals detected on the cell surface. Taken together, these results demonstrate that HepRNA alone can recruit KIR2DL5 on the cell surface, whereas PVR alone only weakly binds to soluble KIR2DL5. The data supports the model that HepRNA functions as a co-receptor for KIR2DL5, and thereby facilitates its engagement with PVR.

Discussion

We have established a novel probe to investigate csRNA by exploiting the broad RNA-binding activity of TLR7 ectodomain fused with Fc tag. Using this probe, we have gained a mechanistic understanding of csRNA presentation through a pooled genome-wide screening, which resulted in the identification of heparan sulfate as an essential molecular factor for the presentation of RNA on the cell surface. We also uncovered that a set of RBPs stably associated with the plasma membrane can serve as a bridge between HepRNA and heparan sulfate. We further unveiled that cell surface glycoproteins such as PVR were adjacent to HepRNA, and demonstrated that one of PVR's known interactors, KIR2DL5, can be enriched on the cell surface by HepRNA, likely supporting efficient binding to PVR.

Heparan sulfate as a scaffold for RNA and RBP. Our study offers insights into the molecular configuration for RNA and RBP presentation on cell surface in living cells. While direct interaction between carbohydrates and nucleic acid has been reported,[42] our data supports RBPs as crucial adapter molecules to bridge the two negatively charged biopolymers. Although the RBPs were not identified from the genetic screening, they were significant hits in the HepRNA-proximal proteome. This is likely due to the functional redundancy of these RBPs on the cell surface: knocking out one RBP may have been compensated by others, such that no apparent decrease of HepRNA could be observed using flow cytometry during genetic screening. Our findings are in line with other work in which select RBPs have been independently shown in to access the outer leaflet of plasma membrane. However, how they are associated with the cell surface remained poorly understood. They are typically soluble proteins and thus do not possess a transmembrane domain anchoring them on the lipid bilayer. A recent study has shown the stable association of an RNA helicase U5 snRNP200 with the cell surface relied on protein-protein interaction with the Fc-gamma receptor

IIIA.[9] Here we demonstrated that the protein-HS interaction may constitute an alternative way of RBP cell surface presentation. This interaction may be mediated by a designated HS-binding domain present on the RBP, or a promiscuous RNA-binding domain,[43] which typically harbors positively charged side chains for the electrostatic interaction with HS. La protein, for example, contains a putative HS-binding motif (GRRFKG) at its C-terminus disordered region, implying potential HS-binding activity.[44] Conversely, hnRNPA1 does not contain any HS-binding motif, despite its presence on the cell surface of wildtype, but not on HS-deficient mutant cells, suggesting possible charge interaction between HS and its RNA-binding domains or other portion of the protein.

While the exact molecular arrangement and stoichiometry of HepRNA, RBP, and HS warrant future studies, our data suggests it may involve RNP condensate formation, and that for a stable presentation, HepRNA and RBP are interdependent. Carbohydrate-protein interactions are generally weak (micromolar to millimolar K_D),[45, 46] and having multiple binding sites is a typical strategy of carbohydrate-binding proteins to overcome such intrinsically low affinity, and stay bound avidly to carbohydrates, which is known as the multivalency effect.[47] In the case of RBPs as HS-binding proteins, the multivalency is brought about likely when several RBPs, either homogeneous or heterogeneous, form complexes with RNA, thus strengthening avidity of the RNP complexes for HS. This is implied by the observation that upon treatment with RNase, the csRNA signal given rise to by anti-La protein staining dropped considerably, likely due to the disassembly of the RNP complexes, and dissociation of RBPs from the HS scaffold, caused by RNA degradation. Future studies should focus on defining the molecular composition of the HS-associated RNP complex.

HepRNA as a co-binder to modulate cell surface ligand-receptor interactions. We further demonstrate that once displayed on the cell surface, the RNA can modulate the interaction of adjacent glycoproteins with their binders. In the case of the PVR-KIR2DL5 interaction, HepRNA functions as a co-binder, recruiting KIR2DL5 to PVR-proximal sites, facilitates PVR engagement, and compensates for the weak affinity of PVR for KIR2DL5.[40] The co-binder effect in modulating cell surface receptor-ligand interactions is not uncommon. For example, the engagement of fibroblast growth factor 2 (FGF-2) with FGFR requires the former to engage with HS, likely resulting in a liquid-liquid phase separation.[48] KIR2DL5, together with a few other KIR family members, has been previously shown to bind to heparin in-vitro via the d0 domain, which is rich in positively charged amino acids.[49] Heparin is often considered a molecular mimicry of nucleic acids because of its heavy negative charges along the polysaccharide chain and has been used to purify select nucleic acid-binding proteins. Although binding to heparin in-vitro, the sensitivity of KIR2DL5-Fc binding towards RNase suggests it may be directly interacting with HepRNA, at least partly, on living cell surface. Notably, such promiscuity has been described for a cell-surface-localized

protein, RAGE, which was previously shown to bind to HS,[50] and more recently also to DNA,[51] as well as for certain antibodies directed against DNA, which can cross-react with HS.[52, 53]

Origin of HepRNA. One key question remains as to the origin of the HepRNA and the associated RNA-binding proteins. While they could be secreted from neighboring and/or distant cells or the cell debris ("outside-on"),[54] the transport of intracellular ribonucleoproteins to the plasma membrane of the same cell ("inside-out") is equally likely. In the "outside-on" model, RNPs can be directly deposited on the HS chains, thereby getting stably displayed on the cell surface. The "inside-out" model requires the translocation of cytosolic RNA and RBPs to the luminal side of specific membraneous organelles. Interestingly, a recent study from Ren et al.[55] showed a distinct set of RNAs from the cytosolically localized transcripts can be found in the ER lumen, implying an unidentified pathway for RNA luminal translocation. In our genetic screening study, TMED10 was identified as an essential factor for HepRNA presentation. This multifunctional protein forms channels on the ERGIC membrane and mediates the translocation of select cytosolic proteins without leader peptide to the luminal side of the vesicle for secretion.[56] Of particular interest, TMED10 was reportedly not relevant to HS biosynthesis[57] and has been documented to potentially bind RNA in the RBP2GO database (RBP2GO),[36] implicating their possible roles in vesicular RNA transport.

Conclusion

Our study establishes a crucial link between HS, cell-surface RNAs, and RNA-binding proteins, shedding light on the intricate processes governing the csRNA presentation. While our findings provide valuable insights into the involvement of HS in binding both csRNA and csRBPs, further research is needed to unravel the precise intracellular mechanisms facilitating csRNA transport to the cell surface. Understanding the specific cellular compartments responsible for imparting identity to csRNAs within the vast pool of cellular RNAs is a key avenue for future exploration. This work not only advances our knowledge of cell surface biology but also opens new avenues for investigating the interplay of csRNAs with extracellular ligands, potentially influencing diverse cellular processes.

Author Contributions

Z.L., C.J. and V.R. conceived the study. C.J. and V.R. jointly supervised the studies. Z.L. performed flow cytometry, UV-crosslinking and immunoprecipitation of RNA experiments. B.S.J. performed immunofluorescence imaging experiments. B.S.J., E.B. and T.S. performed EM imaging. Z.L. and R.W. performed genome-wide screening. R.W. processed and analyzed deep sequencing data. R.W. and B.S.J. produced heparan sulfate-deficient mutant cells. Z.L. and I.S.-B. performed TLR7-Fc-proximity biotinylation experiments. I.S.-B. performed LC-MS sample preparation. Z.L. and I.S.-B. performed proteomics data processing and analysis. M.S. produced PVR-knockout mutant cells.

M.V. supervised the proteomics study. M.T. and G.-J.B. provided critical input and suggested useful resources for the study. Z.L., B.S.J. and C.J. co-wrote the manuscript with input from all authors.

Acknowledgements

T.S, V.R. and C.J. was supported by TU Delft-Leiden Health Initiative. C.J. was supported by ERC Consolidator grant (819299) of the European Research Council and Frontier 10-10 (Ewha Womans University). Z.L. was supported by NWO Veni talent program (VI.Veni.222.272).

M.V. is part of the Oncode Institute, which is partly funded by the Dutch Cancer Society (KWF).

Materials and Methods

Cell culture

Mel526, U2OS and HeLa cells were cultured in DMEM (Thermo Fisher Scientific, 31966047) supplemented with 10% Fetal Bovine Serum (FBS, HyClone, SH30071.03HI) and 1x Penicillin-Streptomycin-Glutamine (Thermo Fisher Scientific, 10378016, 100x) at 37℃ with 5 % CO_2. Wild-type Chinese Hamster Ovarian (CHO) (CHO-K1, ATCC, CCL-61) and heparan sulfate deficient mutant cell lines - CHO pgsA-745 and pgsD-677 (ATCC, CRI-2242 and -2244, respectively) were cultured in Ham's F-12K medium (Thermo Fisher Scientific, 21127022) supplemented with 10% FBS and 1x Penicillin-Streptomycin and Glutamine at 37℃ with 5 % CO_2. To minimize possible influence from components in bovine serum, Mel526 cells and the mutant cells were also adapted into 1x Penicillin-Streptomycin-Glutamine-supplemented DMEM containing 1% FBS and 9% chemically defined serum replacement (Panexin CD, Pan-Biotech, P04-93100), following the protocol suggested by the supplier. Prior to experiments, cell culture flasks or dishes were replenished with DMEM containing 10% Panexin-CD without FBS.

Immunocytochemistry

Cells were fixed 24 hours post-seeding in μ-Slide 8 Well Glass Bottom ibidi chambers (ibidi, 80827, ~30,000 cells/well) with 4% Paraformaldehyde (PFA) aqueous solution (Electron Microscopy Sciences, 15710-S) in PBS for 10 min at RT and washed with PBS twice. Blocking was performed with blocking buffer containing 3% Bovine Serum Albumin in PBS (Sigma, A7638) for 1 hour at RT in RNase-free conditions by adding SUPERaseIn™ RNase Inhibitor (Thermo Fisher Scientific, AM2696, 1:200). For RNA competition, a synthetic RNA oligo (Dharmacon™) with a sequence 5'-pGUCUUCAAAACUAGGUCGUUUUAGA-3'/biotin/ was added at 10 μM during TLR7-Fc incubation. For RNase-treated samples, RNase Cocktail™ Enzyme Mix (Thermo Fisher Scientific, AM2296, 1:100) was added to the blocking buffer. Post-blocking, recombinant proteins or primary antibodies were added to cells prepared in the same respective blocking buffer and incubated at 21℃ for 1 hour. Cells were washed 3 times with PBS (2 minutes per wash) followed by the addition of secondary antibodies prepared in the blocking buffer along with DAPI (Roche, 10236276001, 1 μg/mL final concentration) and incubated at 21℃ for 1h. The cells were washed with PBS and imaged with confocal microscopy (Olympus A1R SiM, oil immersion, filter settings for Red (Alexa-546 and others: excitation 551nm, emission 565 nm); Blue (DAPI: excitation 358 nm, emission 463 nm); Green (Alexa-488 and others: excitation 490nm, emission 544nm) and Far-red (Alexa-647 and others: excitation 650 nm, emission 671 nm).

Electron microscopy

U-2 OS cells were cultured in a 6 cm petri dish at 90-100% confluency. To avoid fixation-induced artefacts, live cells were first stained for csRNA by incubating on ice for 30minutes and then applying TLR7-Fc (3% Bovine Serum Albumin in PBS, final conc 2.5 μg/mL) for 1 hour on ice

followed by thorough washing and incubation with PAG-10 (Protein-A-gold 10nm, PAG10 nm/S, OD50 ,Cell Microscopy Core, UMC Utrecht) solution in PBS (1:50) on ice for 30minutes. Immunogold-labelled cell monolayers were fixed in 1.5% glutaraldehyde in 0.1 M sodium cacodylate buffer for 2 hours before being successively incubated in 1% osmium tetroxide in 0.1 M cacodylate buffer for 1 hour and in 1% uranyl acetate in water for 1 hour. The cells were then dehydrated through a series of incubations in ethanol (70-100%) for 90 minutes and embedded in Epon. The flat embedded cells were sectioned with an ultramicrotome (UC6, Leica, Vienna) using a 35 degrees diamond knife (Diatome, Biel, Switzerland) at a nominal section thickness of 70 nm. The sections were transferred to a formvar and carbon coated 200 mesh copper grid and stained for 20 minutes with 7% uranyl acetate in water and for 10 minutes with lead citrate. EM images were recorded using a Tecnai 12 electron microscope (Thermo Fisher Scientific) equipped with an EAGLE 4k×4k digital camera. For navigation on EM images, montages of images at 11,000× were generated using stitching software.[58] The stitched images were imaged and annotated using Aperio ImageScope (Leica Biosystems).

Flow cytometry analysis of csRNA on live cells

Cells cultured to 80-90% confluency were washed once with 1x DPBS after removing culture media, and then lifted with 10 mM EDTA (diluted from 0.5M sterile filtered stock solution) in 1x DBPS at 37 ℃ for 5 minutes. Lifted cells were dispensed into a 96-well FACS plate with 2-2.5 x10^5 cells per well. For extracellular RNase treatment, PureLink RNase A (Thermo Fisher Scientific, 12091021) were added to the lifting buffer at a final concentration of 40 μg/mL. After spinning down at 300 g for 5 minutes at 4℃ and supernatant removal, cells in each well were resuspended in 30 μL of TLR7-Fc or other Fc-tagged proteins (final concentration 5 μg/mL) in 0.5% BSA in 1x DPBS containing 200U/mL RNasein (Promega, N2511), and incubated on ice for 45 minutes. For secondary only control, cells were incubated with 30 μL 0.5% BSA in 1x DPBS. After incubation, 200 μL cold 1x DBPS were added to each well and the plate was spun down at 300 g for 5 minutes at 4℃. After supernatant removal, cells were resuspended in 30 μL of goat-anti-human IgG AlexaFluor647 conjugate (Thermo Fisher Scientific, A-21445) in 0.5% BSA in 1x DPBS, and incubated in dark for 30 minutes on ice. Upon completion, 200 μL cold 1x DBPS were added to each well and the plate was spun down at 300 g for 5 minutes at 4℃. Finally, cells were resuspended in 200 μL cold 0.5% BSA in 1x DPBS containing 0.1 μg/mL DAPI. The cells were then analyzed on a flow cytometer using HTS settings. Typically, 150 μL cell suspension per well was infused in the system for analysis, with a flow rate of 1 mL/minute. See **Supplementary Fig. 3** for a typical gating method for live, single cells.

TLR7-Fc binding rescue by exogenous RNA

Cells were processed as was described above, except for that after detachment with EDTA buffer containing Purelink RNase A, cells were spun down, resuspended in 1x DPBS containing 200

U/mL RNasein, with varying concentration of total cellular RNA (2 – 0.2 mg/mL), incubated at 4 ℃ for 30 minutes, and washed with cold 1x DPBS, before incubating with TLR7-Fc. The rest of the steps followed exactly the above flow cytometry experiment.

TLR7-RNA crosslinking, precipitation, and on-bead RNA labelling

The procedure after TLR7-Fc binding follows that of eCLIP with modifications.[26] Cells in a 15 cm dish at 90% confluency were washed once with 1x DPBS following culture media removal, and was then incubated with 3 mL per dish 10 mM EDTA in 1x DPBS at 37℃ for 5 minutes. Another 7 mL 1x DPBS was added to the dish to wash cells off the dish. The total of 10 mL cell suspension was transferred to a 15 mL Falcon tube. The dish was washed further with 5 mL 1x DPBS, which was then combined in the same tube. The cells were spun down at 300 g for 5 minutes at 4℃, and the supernatant was removed. The cell pellets were taken up in 250 µL TLR7-Fc (final concentration 5 µg/mL) in 0.5% BSA in 1x DPBS containing 200U/mL RNasein, and the suspension was put on ice for 30 minutes, with gentle tapping every 10 minutes. The tube was topped up to 15 mL with cold 1x DPBS, and spun down at 300 g for 5 minutes at 4℃. The pellets were washed twice with 10 mL cold 1x DPBS. The cells in the second wash were directly transferred to a 10 cm dish for UVC crosslinking on ice without the lid using Stratalinker (400 mJ setting). After UVC exposure, cells were transferred back to the tube and spun down. For TLR7 non-crosslinked control, cells after lifting were transferred into a 15 mL Falcon tube and spun down, resuspended in 10 mL 1x DPBS, and transferred to a 10 cm dish for crosslinking. After crosslinking, cells were transferred back to the 15 mL tube and spun down, and incubated with the TLR7-Fc solution, which was followed by two washes.

The pellets from above were lysed in 400 µL lysis buffer (50 mM Tris-HCl pH 7.4, 100 mM NaCl, 1% v/v Igepal CA-630, 0.1% v/v SDS, 0.5% w/v sodium deoxycholate) containing 1x cOmplete™ protease inhibitor (Roche, 11836153001) cocktail and 1mM PMSF. The solution was sonicated at 20% power for 5 minutes (10s on, 10s off) on ice. To the sonicated lysate was added 2 µL TURBO™ DNase (Thermo Fisher Scientific, AM2238), and 4 µL diluted RNase I (Thermo Fisher Scientific, AM2294, prediluted 1:20 in 1x DPBS). The lysate was then incubated at 37℃ for 5 minutes, followed by the addition of 4 µL SUPERaseIn™. To prepare magnetic beads for TLR-Fc precipitation, 10 µL per dish protein A Dynabeads™ (Thermo Fisher Scientific, 10001D) was washed twice with lysis buffer before added to the above RNA-fragmented lysate. The bead suspension was incubated on an end-to-end rotator at 4 ℃ for 2 hours. The beads were then wash twice with 200 µL CLIP high salt buffer (50 mM Tris-HCl pH 7.4, 1 M NaCl, 1% Igepal CA-630, 1 mM EDTA, 0.1% SDS, 0.5% sodium deoxycholate), three times with 200 µL CLIP low salt buffer (20 mM Tris-HCl pH 7.4, 10 mM $MgCl_2$, 0.2% Tween-20, 5 mM NaCl). The precipitated RNA-TLR7-Fc was 3'-end repaired on-bead by incubating with FastAP (Thermo Fisher Scientific, EF0654, 1 U), T4 PNK (NEB, M0201, 20 U), TURBO™ DNase (0.4 U) and SUPERaseIn™ (5 U) in 10 µL 1x

PNK buffer without DTT at 37 ℃ for 30 minutes, followed by the same wash procedure. The end-repaired RNA was subjected to on-bead 3'-end biotinylation by incubating with 20 nM pCp-biotin, T4 RNA ligase high-concentration (NEB, M0437M, 30 U) and SUPERaseIn™ (5 U) in 1x RNA ligase buffer without DTT, containing 1 mM ATP, 3.6% DMSO, 0.025% Tween-20 and 18% w/v PEG-8000 16 ℃ overnight, which was followed the same wash procedure. After the final wash, beads were directly taken up in 1x LDS sample loading buffer containing 1x sample reducing solution, denatured at 75 ℃ for 10 minutes. The samples were resolved on an NuPAGE™ 4 -12% bis-Tris mini protein gel, wet transferred onto a nitrocellulose (NC) membrane at 30 V for 4 hours at 4 ℃, and subjected to chemiluminescent biotinylated nucleic acid detection. The same NC membrane was finally subjected to Western blot for TLR7 detection using rabbit anti-human TLR7 (1:1000) in combination with horse radish peroxidase (HRP)-conjugated goat-anti-ribbit secondary antibody (1:5000).

Proximity biotinylation of csRNA-proximal proteome

The experiment was performed using three independent cell cultures for each treatment. Cells in a 15 cm dish at 90% confluency were washed twice with 1x DPBS after removing culture media, and was lifted with 3 mL per dish 10 mM EDTA in 1x DPBS. For csRNA-digested sample, RNase A was added to the lifting buffer at a final concentration of 40 μg/mL. 1x DPBS was used to bring cell suspension to 10 mL, which was transferred to a 15 mL Falcon tube. The dish was washed with 5 mL 1x DPBS, which was combined in the same tube. The cells were spun down at 300 g for 5 minutes at 4℃, and pellets were incubated for 30 minutes at 4 ℃ with per dish 250 μL solution of precomplexed TLR7-Fc (5 μg/mL final concentration) and protein-A-HRP conjugate (Thermo Fisher Scientific, 101023, 7 μg/mL final concentration) in 0.5% BSA in 1x DPBS containing 200U/mL RNasein. For an IgG isotype control, human IgG (Thermo Fisher Scientific, 02-7102) was premixed with protein-A-HRP at the same concentration. Cells were washed three times with cold 1x DPBS, and spun down at 200 g for 2 minutes at 4 ℃ each time. After the final wash, the pellets were resuspended in 1 mL per sample 500 μM biotin-phenol in 1x DPBS, and let sit for 1 minute at room temperature. 1 mL 2 mM hydrogen peroxide in 1x DPBS was added to each sample and mixed well. This mixture was incubated for 2 minutes at room temperature and 10 mL cold quenching buffer (5 mM Trolox + 10 mM sodium ascorbate + 10 mM sodium azide in 1x DPBS) was directly added to the sample. The cells were washed two more times with quenching buffer, and were lysed in 300 μL per sample RIPA buffer (50 Mm Tris pH 7.5, 150 mM NaCl, 0.5% sodium deoxycholate, 0.1% SDS, 1% NP40) containing 1x cOmplete™ protease inhibitor cocktail and 1mM PMSF. The lysate was sonicated to clarity, and was spun down at 21,000 g for 10 minutes at 4℃. An aliquot of the supernatant was taken for WB to detect biotin signal, and the rest was subjected to enrichment of biotinylated proteins.

Sample preparation for LC-MS analysis

The procedure follows the reported one by Santos-Barriopedro et al.[59] The supernatant from the sonicated lysate of proximity biotinylated cells was subjected to bead enrichment with 12.5 µL per sample streptavidin sepharose high-performance beads (Cytiva, 15511301) on an end-to-end rotator for 2 h at RT. The beads were washed 5 times with 500 µL RIPA buffer and 4 times with 500 µL PBS. Biotinylated proteins were eluted from beads with 50 µL elution buffer (2 M Urea, 10 mM DTT, 100 mM Tris pH 8), incubated on a thermoshaker at 1500 rpm for 20 minutes at room temperature. Iodoacetamide (50 mM final concentration) was then added, and the samples were incubated in a thermoshaker at 1500 rpm in dark for 10 minutes at room temperature. 2.5 µL per sample trypsin (0.1 mg/mL stock solution) was then added, followed by incubation in a thermoshaker at 1500 rpm for 2 hours at room temperature. Samples were spun down and the alkylated, trypsinized eluates were collected. Another 50 µL elution buffer was then added to the beads, incubated on a thermoshaker at 1500 rpm for 5 minutes at room temperature, and collected and combined with the first elution. 1 µL per sample fresh trypsin was added and the samples were incubated overnight at room temperature. Tryptic peptides were acidified by adding 10 µL 10% (v/v) TFA, and purified using C18 Stagetips (3M Empore). Peptides bound on the Stagetip were stored at 4 °C until LC–MS analysis.

Proteomics and data analysis

Peptides bound to the StageTips were eluted with 30 ml of elution buffer (0.1% formic acid, 80% acetonitrile), reduced to a volume of 5 ml by Speedvac centrifugation, after which 7 ml of buffer A (0.1% formic acid) was added. Then, 6 ml of each sample was loaded on an Easy LC1000 (Thermo Fisher Scientific) connected online an Orbitrap Exploris 480. An acetonitrile gradient of 12-30% in 43 minutes was used followed by an increase of the acetonitrile concentration to 60% in 10 minutes and to 95% in 1 minute. Acquisition time was 60 minutes and the spray voltage was 2200V in positive ion mode. The full scan of the peptides was set to a resolution of 120,000 in a scan range of 350–1300m/z.

MaxQuant 1.5.1.0 options LFQ, iBAQ and match between runs were used to analyse raw files from the mass spectrometry results and human Fasta file updated in 2017 as search database. Downstream analysis was performed using Perseus 1.5.0.15. Contaminants, reverse hits or only identified by site proteins were filtered from the dataset. The triplicates of each experiment were grouped and only proteins with LFQ value in each of the triplicates and in at least one group were considered. Missing values were imputed using default parameters in Perseus. Statistically enriched proteins were identified using a Student's t-test (FDR < 0.05) between the target and the control. Volcano plots were generated by plotting the –log10 of the p-value against the log 2 fold change. Gene ontology term searches for identified hits were performed using RBP2GO.[36]

Genetic screening and data analysis

For knockout screening, the human CRISPR Brunello genome-wide knockout library was a gift from David Root and John Doench (Addgene 73178). For virus production, HEK 293T cells were transfected with packaging plasmids pRSVrev, pHCMV-G VSV-G and pMDLg/pRRE together with the Brunello plasmid using polyethyleneimine (Polyscience Inc.). Virus was harvested, filtered and 150 million Mel526 melanoma cells (a kind gift from Ramon Arens) were transduced in the presence of 8 µg/ml polybrene (Millipore) at an MOI of 0.3. Transduced cells were selected using puromycin (1 µg/ml) and after seven days, two batches of cells were stained for surface RNA using TLR7-Fc and the lowest 5% of expressing cells were sorted. Cells were grown out and sorted again using the same gating strategy as for the first sort. After this sort, genomic DNA was isolated for both the unsorted and sorted populations and gDNAs were amplified using the established protocol.[60] gRNAs were sequenced using the Illumina NovaSeq6000 and inserts were mapped to the reference. Analysis of gRNA enrichment was done using PinAPL-Py.[61]

Genetic screening hit validation

Hits from the knockout screen were validated using the top scoring gRNAs of each gene, which were cloned into the lentiCRISPR v2 vector (a gift from Feng Zhang, Addgene plasmid no. 52961). Mel526 cells were stably transduced with these gRNAs, selected using puromycin, and pooled knockout cells were used for the analysis. Guide sequences were as follows: EXT2, 5′-CACCGTGGTTAAGCACATCGATGGA-3′; EXTL3, 5′-CACCGAAATGAACCTCGGTAACACG-3′; HS6ST1, 5’-AAACCCGCGAGACTTGGCTCTTCTC-3’, C3orf58, 5’-CACCGGCAGACGCACGTCGCCGTTG-3’. Mutant cells were subjected to flow cytometry analysis to check for TLR7-Fc binding, following the procedure described above.

Preparation of PVR KO mutant cells

HEK293T cells (ATCC CRL-3216) were seeded into a 10 cm dish per plasmid at a confluency of 60-70% for lentiviral packaging. The utilized guide RNA was 5’-ATTGGTGCCCTCAAGCCAGG-3’ (PVR, NM_006505.4, NC_000019.10. Sense, exon. Position: 44650019). For a 10 cm dish, 5.63 µg pCMV-VSVG, 8.55 µg pMDLg-RRE (gag/pol), 4.5 µg pRSV-REV and 11 µg pRRL were combined with serum-free DMEM to a total volume of 500 µl. In a second tube, 90 µg of PEI for a 10 cm dish was mixed with serum-free medium to a total volume of 500 µl. This mixture (tube two) was then slowly added to tube one and thoroughly mixed. After 15-30 minutes, the resulting mixture was added dropwise to the cells after adding 4 ml of serum-free medium. 4 hours post-transfection, 4 ml of DMEM with 20% FCS was supplemented to the plate. Subsequently, the plates were incubated overnight at 37°C with 5% CO_2. 48 hours post-transfection, the supernatant containing virus was harvested by collecting the medium into a sterile 15 ml tube. The collected medium centrifugated at 3000 rpm at 4°C for 10 minutes and was subsequently filtered through a 0.45 µm low protein binding membrane (Millipore). The viruses were utilized immediately or stored at -80°C. The transduced cells were cultured using high glucose DMEM with 10% FBS and 1%

Pen-Strep. Transduction was executed by adding 30% of lentivirus plus 5 μg/mL Polybrene. Transduced cells were selected using puromycin (3 μg/ml) 48 hrs after transduction.

FIGURES

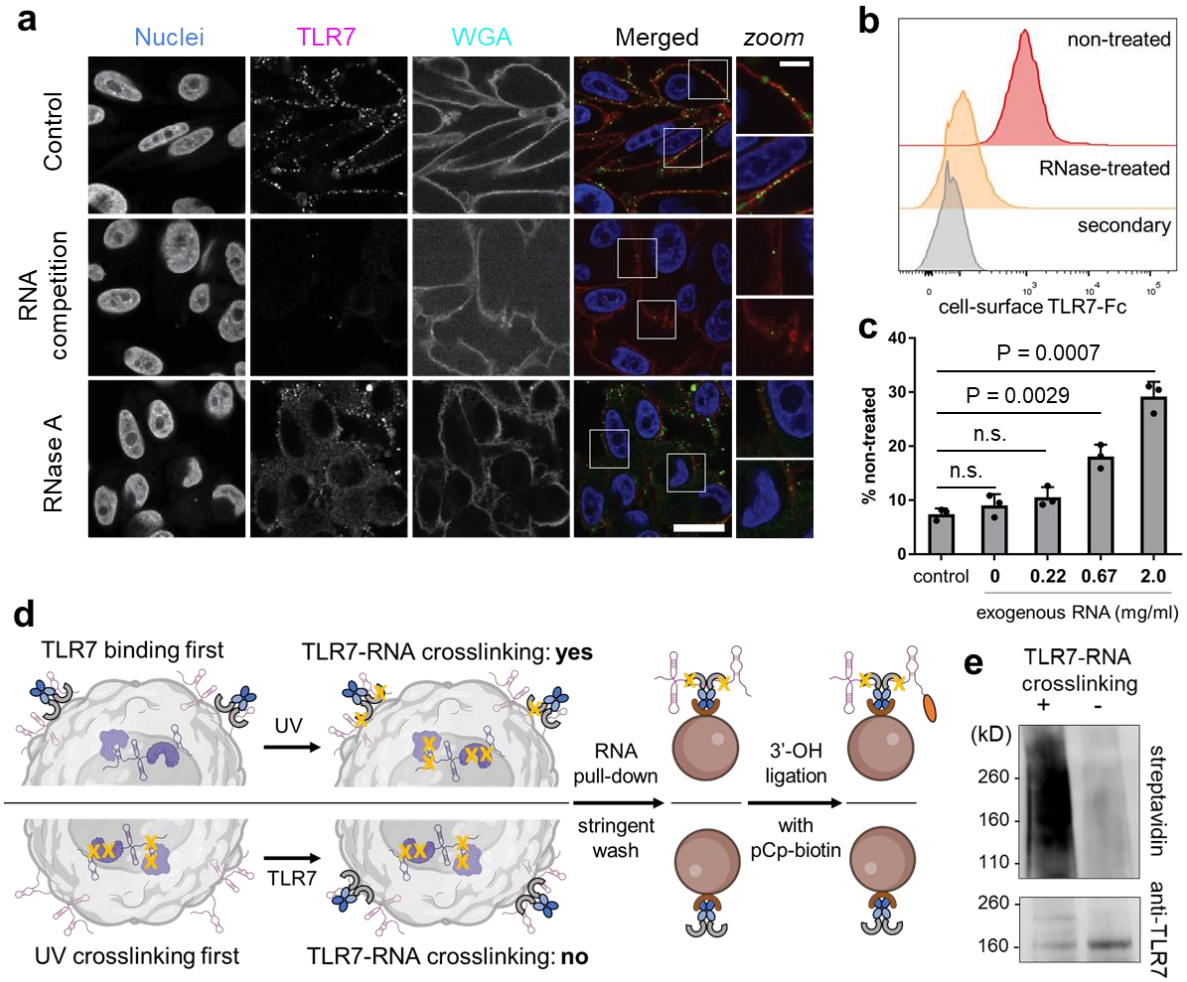

Figure 1. TLR7-Fc probe the cell-surface RNA. a, Representative confocal microscopy images of csRNA on Mel526 cells probed by TLR7-Fc and Alexa Fluor® 488-conjugated Goat-anti-human IgG. Cell surface was stained by WGA-biotin and streptavidin-Alexa Fluor® 594. See supplementary information for the sequence of competitor ssRNA. RNase A concentration, 40 µg/ml. Nuclear counterstaining: DAPI. Scale bar: 20µm. **b**, Flow cytometry analysis of csRNA on Mel526 cells probed by TLR-Fc in complex with goat-anti-human-AlexaFluor647. 40 µg/ml RNase A was used to deplete csRNA during EDTA lifting. n = 3 independent cell cultures. two-tailed Student's t-test, mean ± s.d. **c**, TLR7-Fc binding was rescued by exogenous total RNA in a concentration-dependent manner. n = 3 independent cell cultures. Exogenous RNA in 1x DPBS was added to cells at 4 ℃. 0 mg/ml RNA means 1x DPBS buffer without RNA. The control was with cells treated with RNase A but without any additional incubation. Y-axis shows relative signal intensity, with the geometric mean of TLR7 binding on non-RNase treated cells set to 100%. Two-tailed Student's t-test, mean ± s.e.m. **d**, Schematics of in-situ crosslinking and csRNA capture experiment. Abbreviations: UV, ultraviolet; pCp, cytidine-5'-phosphate-3'-(6-aminohexyl)phosphate. **e**, Chemiluminescent detection of TLR7-captured and biotin-labeled RNA. Rabbit-anti-TLR7 was used to check for TLR7-Fc on the same nitrocellulose membrane after blotting biotinylated RNA. A representative image is shown here. n = 3 independent cell cultures for crosslinked and non-crosslinked samples.

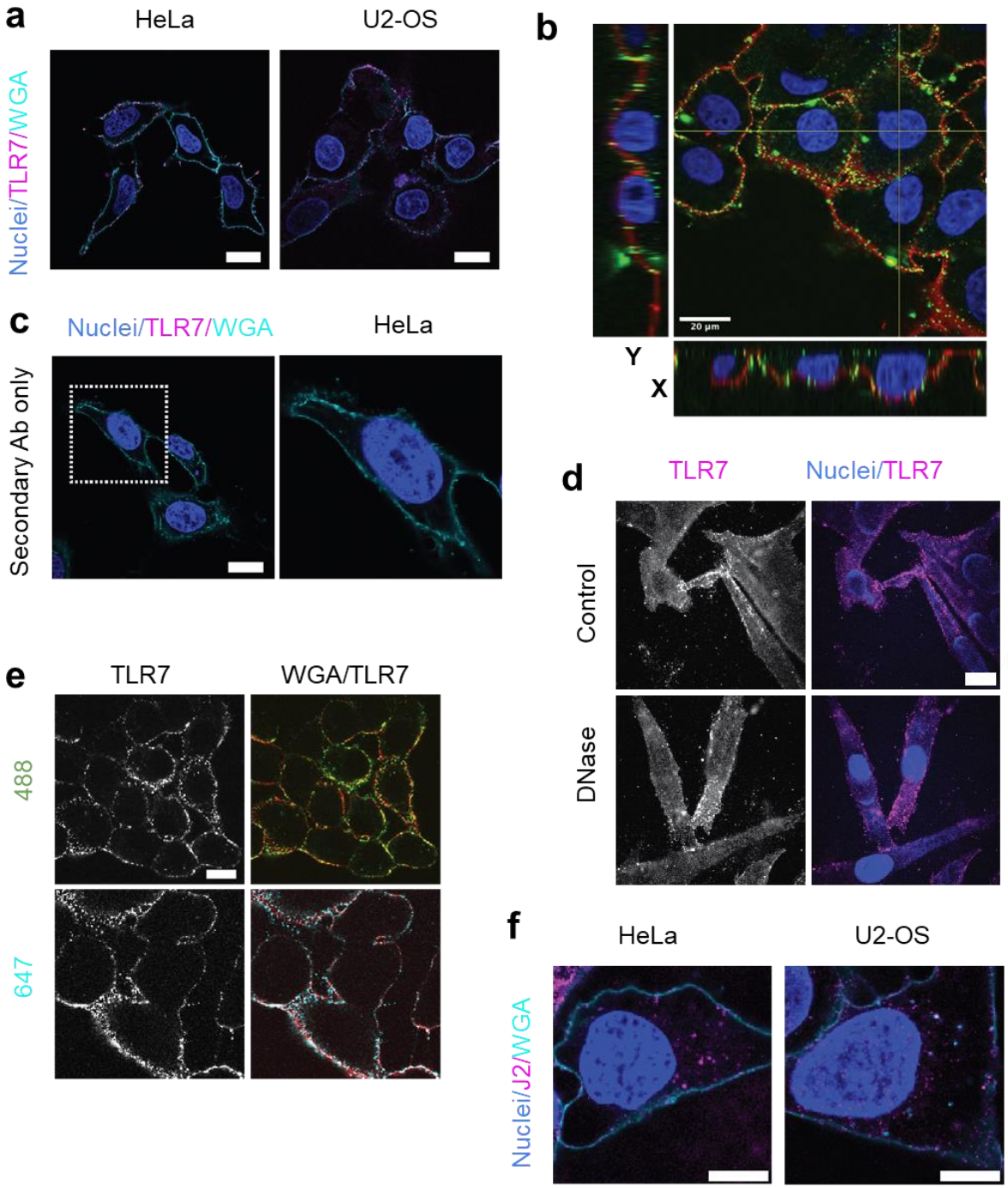

Supplementary Figure 1. Immunofluorescence imaging on different cell lines using TLR7-Fc. a, csRNA staining on HeLa and U2-OS cells probed by TLR7-Fc and Alexa Fluor® 647-conjugated Rat-anti-human IgG Fc antibody (HeLa) or Alexa Fluor® 488-conjugated Goat-anti-human IgG Fc antibody pseudocoloured as magenta (U2-OS). Cell surface was stained by WGA-biotin and streptavidin-Alexa Fluor® 488 (HeLa) or streptavidin-Alexa Fluor® 594, pseudocoloured as green (U2-OS). **b**, Optical sections through U2-OS cells labeled for csRNA with TLR7-Fc and Alexa Fluor® 488-conjugated Rat-anti-human IgG Fc antibody (pseudocoloured magenta) that shows the occurrence of csRNA on the cellular surface. Cell surface was stained by WGA-biotin and streptavidin-Alexa Fluor® 594 (pseudocoloured green). **c**, Representative confocal microscopy images of secondary antibody control (U2-OS

cells) i.e. without TLR7-Fc but with Alexa Fluor® 647-conjugated Rat-anti-human IgG Fc antibody. Inset shows enlarged view. **d**, csRNA staining in the presence or absence of DNase I (10 U/ml) on Mel526 cells probed by TLR7-Fc and Alexa Fluor® 647-conjugated Rat-anti-human IgG Fc antibody. **e**, csRNA staining on living cells incubated at 4^0C with TLR7 and two different secondary antibodies in U2-OS cells (Alexa Fluor® 488- or Alexa Fluor® 647-conjugated anti-human IgG Fc antibodies. **f**, Representative images of double-stranded RNA staining on HeLa and U2-OS cells probed by the J2 antibody and Cy3-conjugated Donkey-anti-mouse IgG. Cell surface was stained by WGA-biotin and streptavidin-Alexa Fluor®488. Nuclear staining: DAPI. Scale bars: 10μm (**a**), 20μm (**b**- **f**).

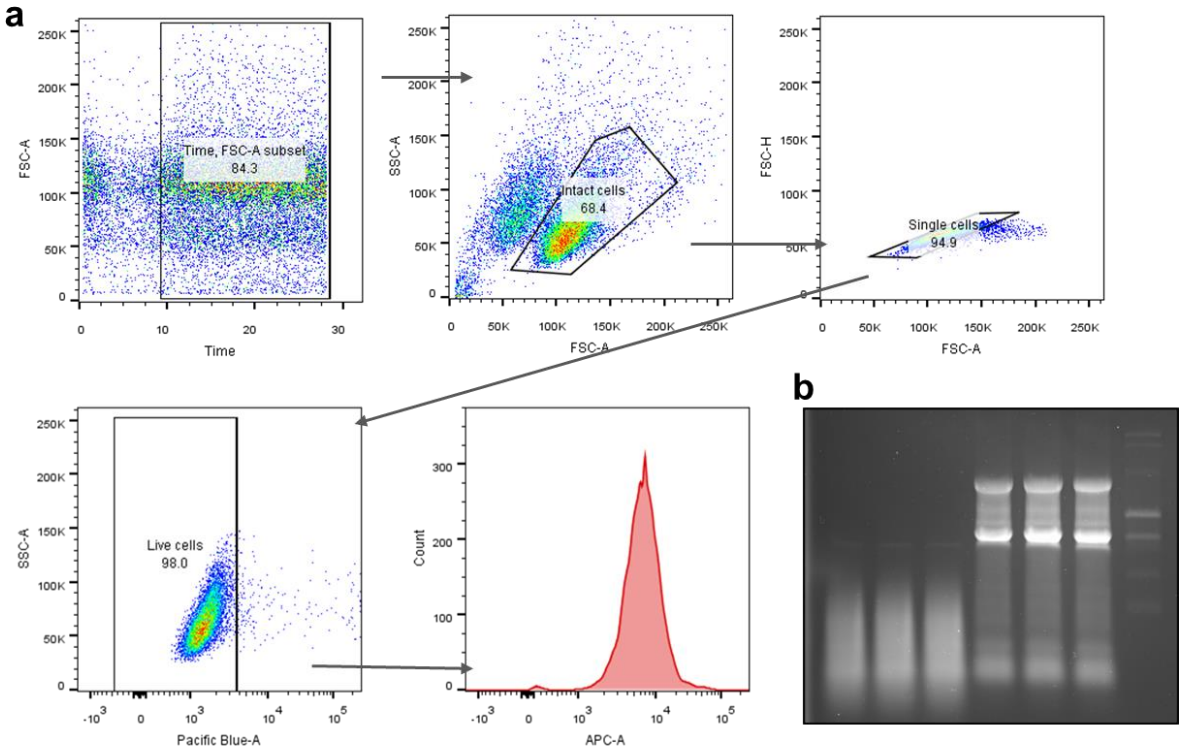

Supplementary Figure 2. Flow cytometry analysis of TLR7-Fc probed cells and binding rescue experiment. a, Gating strategy for TLR7-Fc probed cells in flow cytometry. b, 1% agarose gel analysis of extracted total RNA. Left three lanes were 2-minute fragmented total RNA (from the right three lanes) using magnesium-based fragmentation buffer.

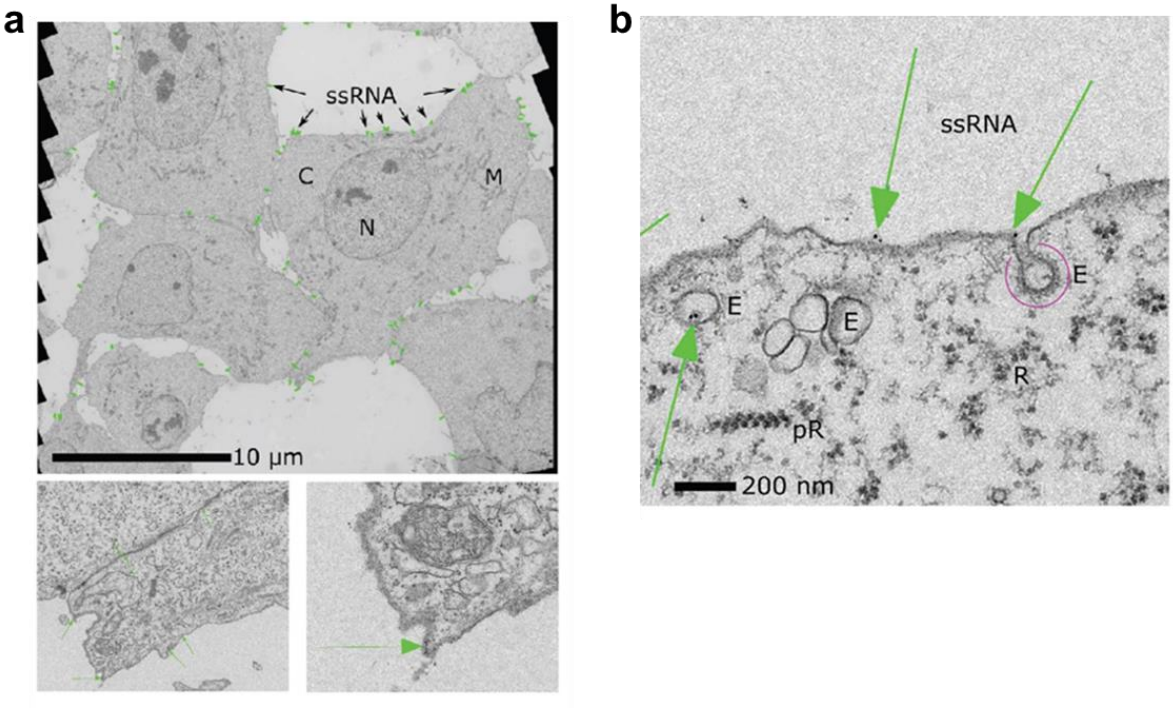

Supplementary Figure 3. Electron microscopy imaging of csRNA using TLR7-Fc. a, The ultrastructure of csRNA localizations in U2-OS cells (green spots + arrows). TLR7-Fc served as a primary probe. 10nm gold nanoparticles conjugated to Protein-A used as a secondary probe provide the necessary contrast in electron microscopic interrogation and can be seen as black dots (green spots and arrows). The bottom panel provides more accounts of csRNA staining. **b**, Some csRNA are internalized into the cell via endocytosis. The green arrow in E indicates the presence of csRNA inside endosome with and without caveolae(pink arc). Abbreviations: C, cytosol; N, nucleus; M, mitochondria, E, endosome, R, ribosome; pR, polyribosome. Scale bars: 10µm (**a**), 200nm (**b**).

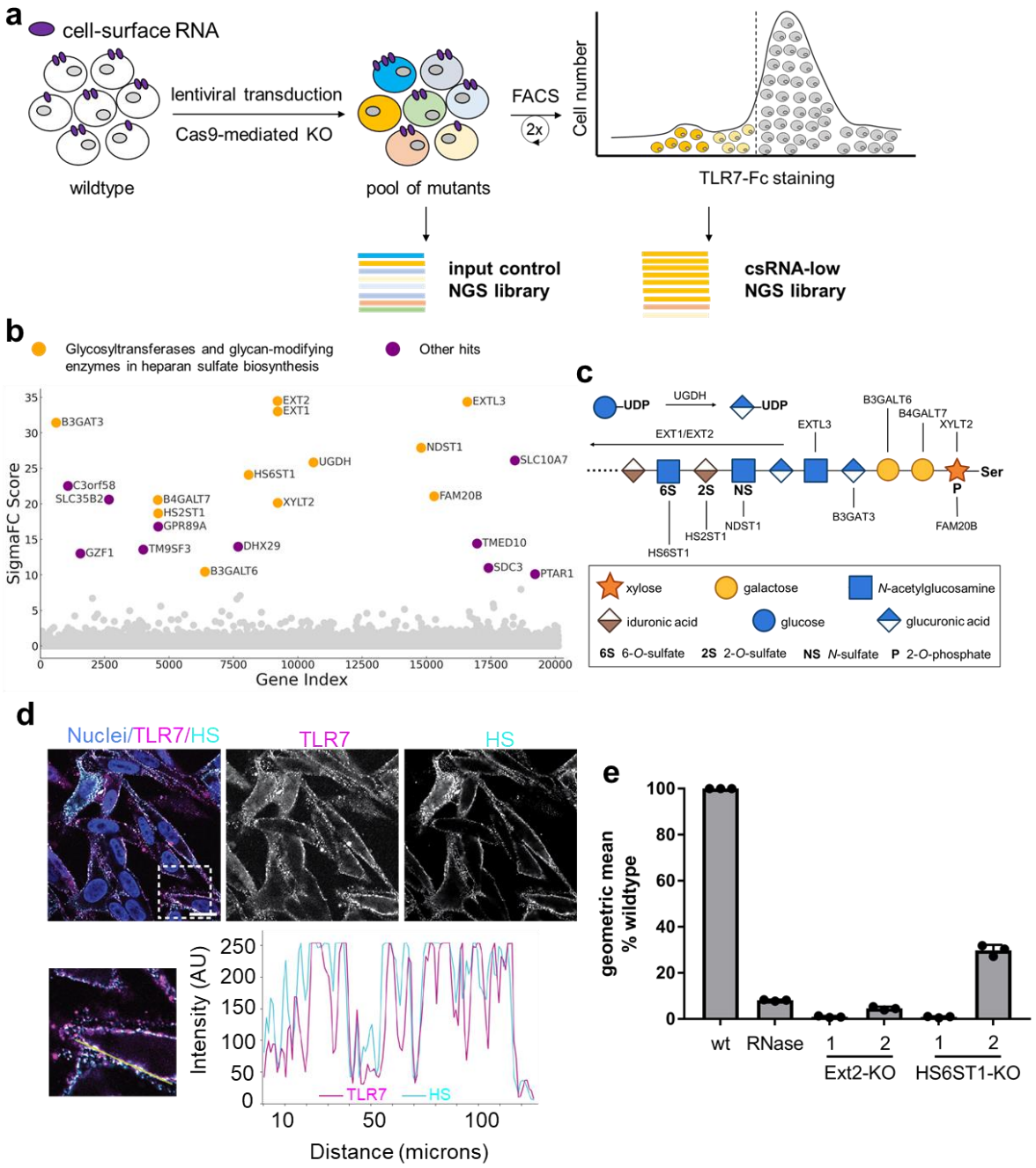

Figure 2. Genome-wide screening reveals essential factors for csRNA stable presentation. a, Schematic of a genetic screen in Mel526 cells using csRNA staining with TLR7-Fc and Alexa Fluor® 488-conjugated Goat-anti-human IgG. Color-coded cells represent the 5% of cells with the lowest fluorescent signal indicating the loss of csRNA. **b**, Dot plot of gene candidates from the screening. SigmaFC scores in this plot are geometric mean of the SigmaFC scores from the duplicates calculated using PinAPL-Py. Heparan sulfate-related glycosyltransferases and glycan-modifying enzymes are colored in yellow. Other hits with a SigmaFC larger than 10 are colored in purple. **c**, Heparan sulfate biosynthetic pathway. Gene candidates as yellow dots in Panel **b** are shown in this schematic representation. **d**, csRNA and HS colocalization on cell surface of Mel526. csRNA is probed by TLR7-Fc and Alexa Fluor®647-conjugated rat-anti-human IgG (magenta), while HS is labeled with mouse anti-HS

(10E4 epitope) antibody and Alexa Fluor® 488-conjugated goat anti-mouse IgM mu chain secondary antibody (cyan). The line intensity profile along the yellow line shows csRNA tightly overlaps with heparan sulfate. Nuclear staining (blue): DAPI. Scale bar: 20 μm. The frame with dashed line indicates the area where intensity profile were collected. **d**, Flow cytometry analysis of csRNA loss in EXT2 and HS6ST1 KO mutant Mel526 cells. TLR7-Fc with goat-anti-human-AlexaFluor647 is used for csRNA staining. 40 μg/ml RNase A treated cells are used as control. The numbers above EXT2 and HS6ST1 represents different guide RNA for KO (see Supplementary Information for sequences). n = 3 independent cell cultures. two-tailed Student's t-test, mean ± s.e.m.

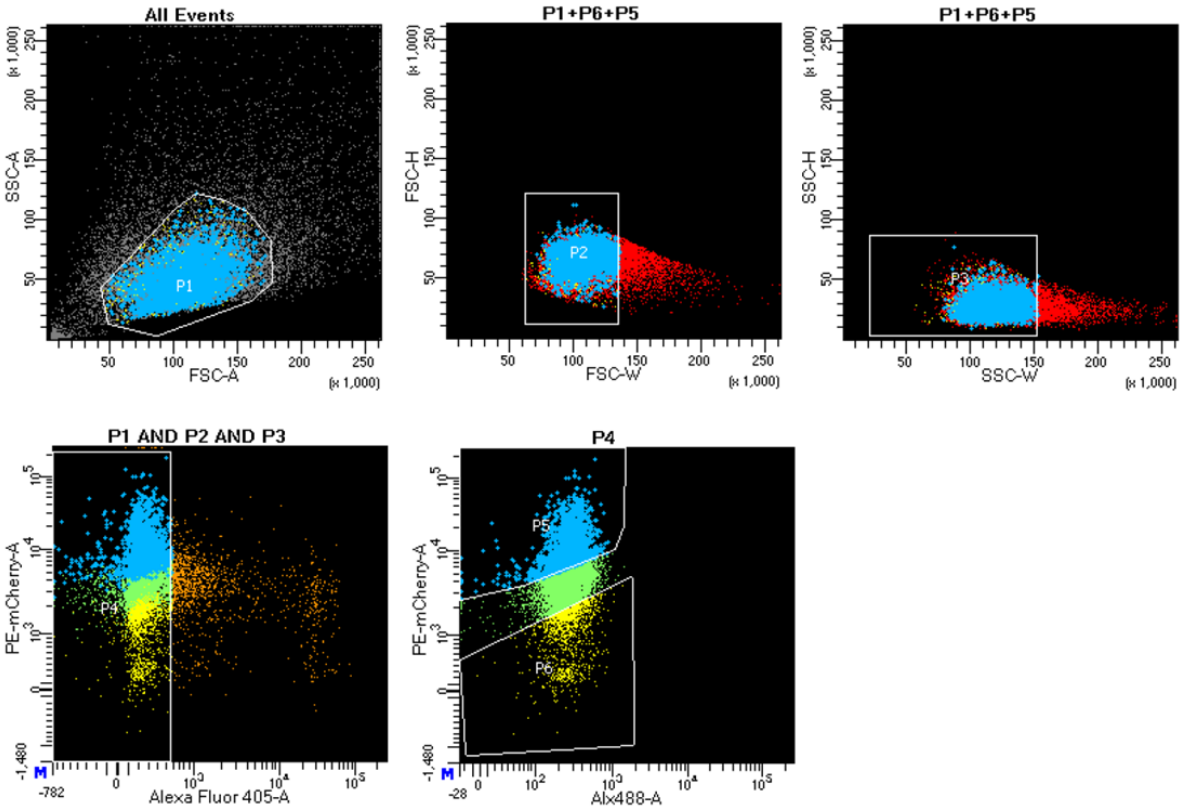

Supplementary Figure 4. Gating strategies in FACS to enrich csRNA-low phenotype among lentiviral transduced cells. P1 gated for intact cells; P2 and P3 gated for singlets; P4 gated for living cells; P6 gated csRNA-low phenotypes.

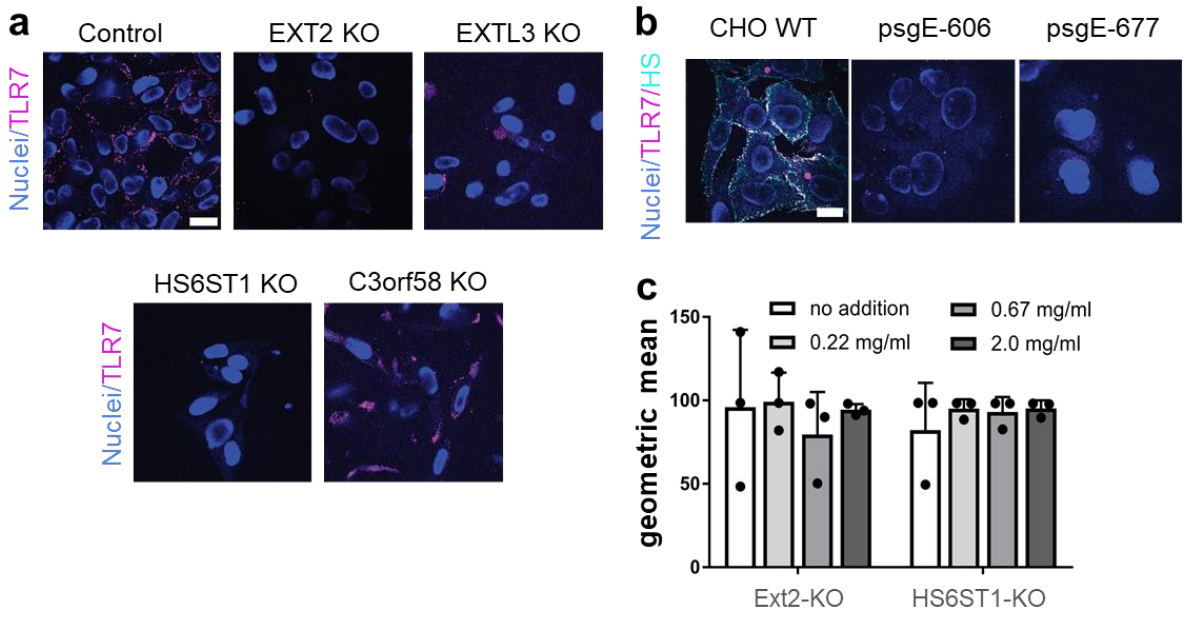

Supplementary Figure 5. Validation of HS as essential factors for cell-surface RNA presentation. a, csRNA staining of EXT2, EXTL3, HS6ST1 and C3orf58 KO mutant cell lines. TLR7-Fc was detected by Alexa Fluor® 488-conjugated goat-anti-human IgG for csRNA (magenta). **b**, csRNA (magenta) and HS (cyan) staining of CHO-K1 (wild type) and heparan sulfate deficient cell lines. The primary secondary antibodies were the same as used in Figure 3d. Nuclear staining: DAPI. Scale bars: 20 µm (**a-b**). **c**, TLR7-Fc binding was not rescued by exogenous total RNA for HS-deficient mutant cells. n = 3 independent cell cultures. None of the groups is significant compared to no-RNA control (the white bar on the left). Two-tailed Student's t-test, mean ± s.e.m.

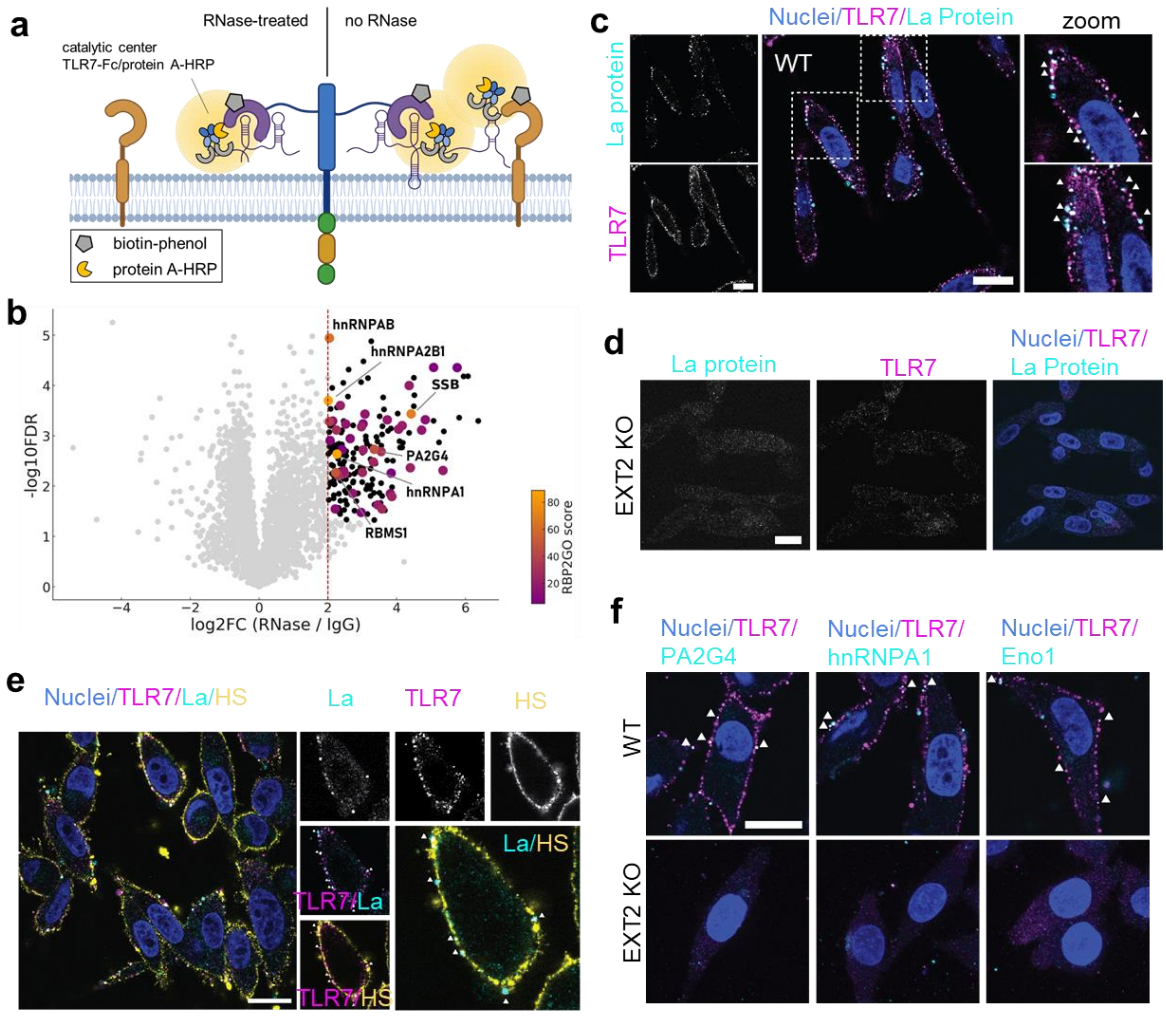

Figure 3. Cell-surface RNA-binding proteins connect HepRNA with HS. a, Schematic representation of TLR7-mediated proximity labeling to identify HepRNA-proximal proteome. Cells probed with TLR7 probe and human IgG control, and extracellularly RNase-treated cells probed with TLR7 were performed in triplicates. **b**, Volcano plot of significantly enriched proteins proximal to TLR7-Fc from extracellular RNase-treated cells over IgG control. RBPs documented in RBP2GO database are shown as larger dots and gradient-colored based on their RBP2GO scores. Names are shown for RBP hits with RBP2GO scores larger than 45. The other hits shown in black with smaller size are enriched protein hits not documented in RBP2GO. Grey dots are not significantly enriched proteins. **c**, Representative images of HepRNA and Lupus La protein on Mel526 cells. Insets indicate zoomed in areas. White arrows show colocalization of HepRNA with the RNA-binding protein. La protein staining was lost in EXT2 knockout cells. 40 µg/ml RNase A treated cells also led to the partial loss of HepRNA and La protein. **d**, HS and La protein colocalization on cell surface of Mel526. **e**, HS, La protein, and HepRNA colocalization on cell surface of Mel526. **f**, Colocalization of HS and RBPs on cell surface of Mel526 and EXT KO. La protein and other RBPs were detected with rabbit anti-RBP antibodies and Cy3-conjugated goat anti-rabbit secondary antibody. Nuclear staining: DAPI. Scale bars: 20µm (**c-f**)

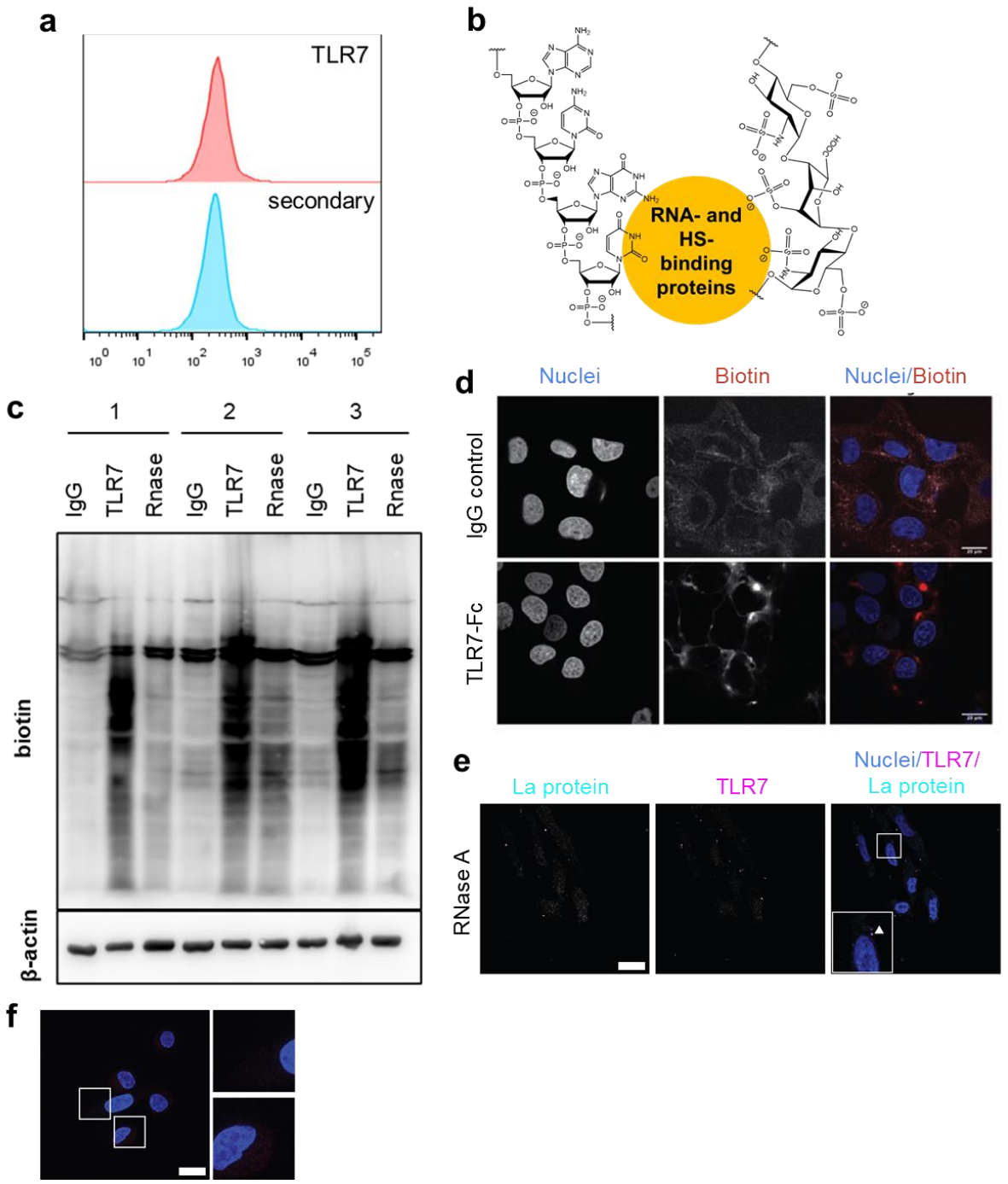

Supplementary Figure 6. Indications for that RNA and HS are bridged with proteins. a, Flow cytometry analysis of proteolytically lifted cells, which lost TLR7-Fc binding. **b**, schematic representation of how RNA and HS, both of which are negatively charged, are bridged by proteins. **c**, Western blot of proximity biotinylated cell surface proteins. IgG, wildtype cells incubated with human IgG isotype control precomplexed with protein A-HRP; TLR7, wildtype cells incubated with TLR7-Fc precomplexed with protein A-HRP; RNase, extracellularly RNase-treated cells incubated with TLR7-Fc precomplexed with protein A-HRP. The numbers above sample names indicate replicates. **d**, Fluorescence images of proximity biotinylation of extracellular RNase-treated cells. IgG was used as a control to check for background labeling. Red foci indicate biotinylation of HepRNA proximal proteins via biotin-phenol in the presence

of HRP and hydrogen peroxide. **e**, Representative images of HepRNA and Lupus La protein on RNaseA treated Mel526 cells. Inset indicates zoomed in area. White arrow shows a single instance of colocalization of HepRNA with the RNA-binding protein. La protein staining was lost in EXT2 knockout cells. 40 μg/ml RNase A treated cells also led to the partial loss of HepRNA and La protein. **f**, Secondary antibody only control fluorescence image of Mel526. Nuclear staining: DAPI.Scale bars: 20μm.

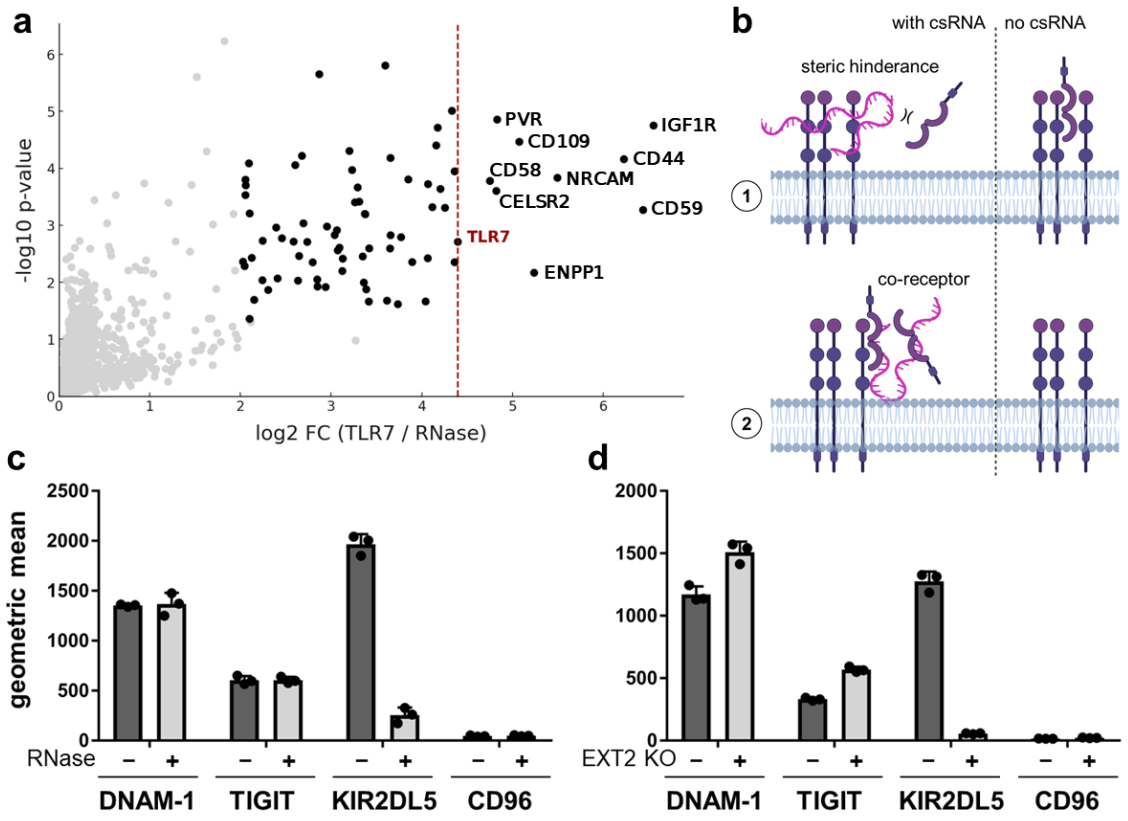

Figure 4. HepRNA modulates membrane receptor-ligand interactions. a, Volcano plot significantly enriched proteins proximal to TLR7-Fc (HepRNA-bound) from wildtype (non-treated) cells over extracellular RNase-treated controls. TLR7 fold of enrichment is used a threshold (indicated by a red dashed line) for selecting protein of interest. **b**, Schematic representation of how HepRNA may regulate ligand-receptor interaction on the plasma membrane. **c**, bar graphs from flow cytometry analysis of live cell surface binding of PVR-binding Fc-fused recombinant proteins, in the presence or absence of HepRNA. 40 µg/mL RNase A was used to deplete HepRNA. Alexa Fluor® 647-conjugated goat-anti-human was used to detect Fc-fused proteins on live cell surface. n = 3 independent cell cultures. **d**, bar graphs from flow cytometry analysis live cell surface binding of PVR-binding Fc-fused recombinant proteins. Wildtype Mel526 and the mutant with EXT2 knockout cells were compared side-by-side. n = 3 independent cell cultures.

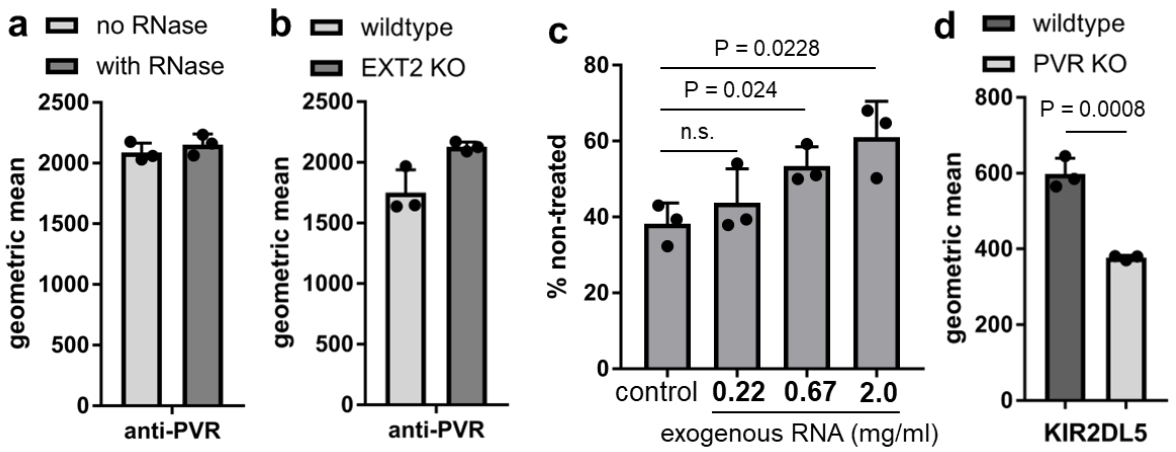

Supplementary Figure 7. HepRNA recruits KIR2DL5 on cell surface. a, Bar graphs from flow cytometry analysis of live cell surface binding of monoclonal anti-PVR antibody, in the presence or absence of HepRNA. Primary antibody was detected by Alexa Fluor® 488-conjugated goat-anti-mouse secondary antibody. n = 3 independent cell cultures. **b**, Bar graphs from flow cytometry analysis of live cell surface binding of monoclonal anti-PVR antibody to wildtype and EXT2-KO mutant Mel526 cells. n = 3 independent cell cultures. **c**, KIR2DL5-Fc binding was rescued by exogenous total RNA in a concentration-dependent manner. n = 3 independent cell cultures. **d**, Bar graphs from flow cytometry analysis of live cell surface binding of KIR2DL5-Fc to wildtype and PVR-KO mutant cells. n = 3 independent cell cultures.

References

1. Block, K. F.; Puerta-Fernandez, E.; Wallace, J. G.; Breaker, R. R. Association of OLE RNA with bacterial membranes via an RNA–protein interaction. *Molecular Microbiology* 2011, **79**(1)**:** 21-34.

2. Flynn, R. A.; Pedram, K.; Malaker, S. A.; Batista, P. J.; Smith, B. A. H.; Johnson, A. G.; George, B. M.; Majzoub, K.; Villalta, P. W.; Carette, J. E.; Bertozzi, C. R. Small RNAs are modified with N-glycans and displayed on the surface of living cells. *Cell* 2021, **184**(12)**:** 3109-3124.e3122.

3. Huang, N.; Fan, X.; Zaleta-Rivera, K.; Nguyen, T. C.; Zhou, J.; Luo, Y.; Gao, J.; Fang, R. H.; Yan, Z.; Chen, Z. B.; Zhang, L.; Zhong, S. Natural display of nuclear-encoded RNA on the cell surface and its impact on cell interaction. *Genome Biology* 2020, **21**(1)**:** 225.

4. Wu, E.; Guo, X.; Teng, X.; Zhang, R.; Li, F.; Cui, Y.; Zhang, D.; Liu, Q.; Luo, J.; Wang, J.; Chen, R. Discovery of Plasma Membrane-Associated RNAs through APEX-seq. *Cell Biochemistry and Biophysics* 2021, **79**(4)**:** 905-917.

5. Hemberger, H.; Chai, P.; Lebedenko, C. G.; Caldwell, R. M.; George, B. M.; Flynn, R. A. Rapid and sensitive detection of native glycoRNAs. *bioRxiv* 2023**:** 2023.2002.2026.530106.

6. Zhang, N.; Tang, W.; Torres, L.; Wang, X.; Ajaj, Y.; Zhu, L.; Luan, Y.; Zhou, H.; Wang, Y.; Zhang, D.; Kurbatov, V.; Khan, S. A.; Kumar, P.; Hidalgo, A.; Wu, D.; Lu, J. Cell surface RNAs control neutrophil recruitment. *Cell* 2024, **187**(4)**:** 846-860.e817.

7. Semenkovich, C. F.; Ostlund, R. E., Jr.; Olson, M. O. J.; Yang, J. W. A protein partially expressed on the surface of HepG2 cells that binds lipoproteins specifically is nucleolin. *Biochemistry* 1990, **29**(41)**:** 9708-9713.

8. Hee Jo, S.; Choi, J.-A.; Lim, Y.-J.; Lee, J.; Cho, S.-N.; Oh, S.-M.; Go, D.; Kim, S.-H.; Song, C.-H. Calreticulin modulates the intracellular survival of mycobacteria by regulating ER-stress-mediated apoptosis. *Oncotarget; Vol 8, No 35* 2017.

9. Knorr, K.; Rahman, J.; Erickson, C.; Wang, E.; Monetti, M.; Li, Z.; Ortiz-Pacheco, J.; Jones, A.; Lu, S. X.; Stanley, R. F.; Baez, M.; Fox, N.; Castro, C.; Marino, A. E.; Jiang, C.; Penson, A.; Hogg, S. J.; Mi, X.; Nakajima, H.; Kunimoto, H.; Nishimura, K.; Inoue, D.; Greenbaum, B.; Knorr, D.; Ravetch, J.; Abdel-Wahab, O. Systematic evaluation of AML-associated antigens identifies anti-U5 SNRNP200 therapeutic antibodies for the treatment of acute myeloid leukemia. *Nature Cancer* 2023, **4**(12)**:** 1675-1692.

10. Gillissen, M. A.; Kedde, M.; Jong, G. d.; Moiset, G.; Yasuda, E.; Levie, S. E.; Bakker, A. Q.; Claassen, Y. B.; Wagner, K.; Böhne, M.; Hensbergen, P. J.; Speijer, D.; van Helden, P. M.; Beaumont, T.; Spits, H.; Hazenberg, M. D. AML-specific cytotoxic antibodies in patients with durable graft-versus-leukemia responses. *Blood* 2018, **131**(1)**:** 131-143.

11. Perr, J.; Langen, A.; Almahayni, K.; Nestola, G.; Chai, P.; Lebedenko, C. G.; Volk, R.; Caldwell, R. M.; Spiekermann, M.; Hemberger, H.; Bisaria, N.; Tzelepis, K.; Calo, E.; Möckl, L.; Zaro, B.; Flynn, R. A. RNA binding proteins and glycoRNAs form domains on the cell surface for cell penetrating peptide entry. *bioRxiv* 2023**:** 2023.2009.2004.556039.

12. Vallet, S. D.; Clerc, O.; Ricard-Blum, S. Glycosaminoglycan–Protein Interactions: The First Draft of the Glycosaminoglycan Interactome. *Journal of Histochemistry & Cytochemistry* 2020, **69**(2)**:** 93-104.

13. Esko, J. D.; Lindahl, U. Molecular diversity of heparan sulfate. *The Journal of Clinical Investigation* 2001, **108**(2)**:** 169-173.

14. Lamanna, W. C.; Kalus, I.; Padva, M.; Baldwin, R. J.; Merry, C. L. R.; Dierks, T. The heparanome—The enigma of encoding and decoding heparan sulfate sulfation. *Journal of Biotechnology* 2007, **129**(2)**:** 290-307.

15. Ma, Y.; Guo, W.; Mou, Q.; Shao, X.; Lyu, M.; Garcia, V.; Kong, L.; Lewis, W.; Ward, C.; Yang, Z.; Pan, X.; Yi, S. S.; Lu, Y. Spatial imaging of glycoRNA in single cells with ARPLA. *Nature Biotechnology* 2024, **42**(4)**:** 608-616.

16. Petes, C.; Odoardi, N.; Gee, K. The Toll for Trafficking: Toll-Like Receptor 7 Delivery to the Endosome. *Frontiers in Immunology* 2017, **8**.

17. Zhang, Z.; Ohto, U.; Shibata, T.; Taoka, M.; Yamauchi, Y.; Sato, R.; Shukla, N. M.; David, S. A.; Isobe, T.; Miyake, K.; Shimizu, T. Structural Analyses of Toll-like Receptor 7 Reveal Detailed RNA Sequence Specificity and Recognition Mechanism of Agonistic Ligands. *Cell Reports* 2018, **25**(12)**:** 3371-3381.e3375.

18. Monsigny, M.; Roche, A.-C.; Sene, C.; Maget-Dana, R.; Delmotte, F. Sugar-Lectin Interactions: How Does Wheat-Germ Agglutinin Bind Sialoglycoconjugates? *European Journal of Biochemistry* 1980, **104**(1)**:** 147-153.

19. Fischer, L. S.; Klingner, C.; Schlichthaerle, T.; Strauss, M. T.; Böttcher, R.; Fässler, R.; Jungmann, R.; Grashoff, C. Quantitative single-protein imaging reveals molecular complex formation of integrin, talin, and kindlin during cell adhesion. *Nature Communications* 2021, **12**(1)**:** 919.

20. Owen, D. M.; Rentero, C.; Rossy, J.; Magenau, A.; Williamson, D.; Rodriguez, M.; Gaus, K. PALM imaging and cluster analysis of protein heterogeneity at the cell surface. *Journal of Biophotonics* 2010, **3**(7)**:** 446-454.

21. Melan, M. A.; Sluder, G. Redistribution and differential extraction of soluble proteins in permeabilized cultured cells Implications for immunofluorescence microscopy. *Journal of Cell Science* 1992, **101**(4)**:** 731-743.

22. Tanaka, K. A. K.; Suzuki, K. G. N.; Shirai, Y. M.; Shibutani, S. T.; Miyahara, M. S. H.; Tsuboi, H.; Yahara, M.; Yoshimura, A.; Mayor, S.; Fujiwara, T. K.; Kusumi, A. Membrane molecules mobile even after chemical fixation. *Nature Methods* 2010, **7**(11)**:** 865-866.

23. Helmreich, E. J. M. Environmental influences on signal transduction through membranes: a retrospective mini-review. *Biophysical Chemistry* 2002, **100**(1)**:** 519-534.

24. Dhir, A.; Dhir, S.; Borowski, L. S.; Jimenez, L.; Teitell, M.; Rötig, A.; Crow, Y. J.; Rice, G. I.; Duffy, D.; Tamby, C.; Nojima, T.; Munnich, A.; Schiff, M.; de Almeida, C. R.; Rehwinkel, J.; Dziembowski, A.; Szczesny, R. J.; Proudfoot, N. J. Mitochondrial double-stranded RNA triggers antiviral signalling in humans. *Nature* 2018, **560**(7717)**:** 238-242.

25. Weber, F.; Wagner, V.; Rasmussen Simon, B.; Hartmann, R.; Paludan Søren, R. Double-Stranded RNA Is Produced by Positive-Strand RNA Viruses and DNA Viruses but Not in Detectable Amounts by Negative-Strand RNA Viruses. *Journal of Virology* 2006, **80**(10)**:** 5059-5064.

26. Van Nostrand, E. L.; Pratt, G. A.; Shishkin, A. A.; Gelboin-Burkhart, C.; Fang, M. Y.; Sundararaman, B.; Blue, S. M.; Nguyen, T. B.; Surka, C.; Elkins, K.; Stanton, R.; Rigo, F.; Guttman, M.; Yeo, G. W. Robust transcriptome-wide discovery of RNA-binding protein binding sites with enhanced CLIP (eCLIP). *Nature Methods* 2016, **13**(6)**:** 508-514.

27. Sanson, K. R.; Hanna, R. E.; Hegde, M.; Donovan, K. F.; Strand, C.; Sullender, M. E.; Vaimberg, E. W.; Goodale, A.; Root, D. E.; Piccioni, F.; Doench, J. G. Optimized libraries for CRISPR-Cas9 genetic screens with multiple modalities. *Nature Communications* 2018, **9**(1)**:** 5416.

28. Marques, C.; Reis, C. A.; Vivès, R. R.; Magalhães, A. Heparan Sulfate Biosynthesis and Sulfation Profiles as Modulators of Cancer Signalling and Progression. *Frontiers in Oncology* 2021, **11**.

29. Kamiyama, S.; Suda, T.; Ueda, R.; Suzuki, M.; Okubo, R.; Kikuchi, N.; Chiba, Y.; Goto, S.; Toyoda, H.; Saigo, K.; Watanabe, M.; Narimatsu, H.; Jigami, Y.; Nishihara, S. Molecular Cloning and Identification of 3'-Phosphoadenosine 5'-Phosphosulfate Transporter. *Journal of Biological Chemistry* 2003, **278**(28)**:** 25958-25963.

30. Durin, Z.; Dubail, J.; Layotte, A.; Legrand, D.; Cormier-Daire, V.; Foulquier, F. SLC10A7, an orphan member of the SLC10 family involved in congenital disorders of glycosylation. *Human Genetics* 2022, **141**(7)**:** 1287-1298.

31. Vanderperre, B.; Muraleedharan, A.; Dorion, M. F.; Larroquette, F.; Del Cid Pellitero, E.; Rajakulendran, N.; Chen, C. X. Q.; Larivière, R.; Michaud-Tardif, C.; Chidiac, R.; Lipuma, D.; MacLeod, G.; Thomas, R.; Wang, Z.; Reintsch, W. E.; Luo, W.; Shlaifer, I.; Fuming, Z.; Xia, K.; Yan, L.; Steinhart, Z.; Linhardt, R. J.; Trempe, J. F.; Liu, J.; Durcan, T. M.; Angers, S.; Fon, E. A. A genome-wide CRISPR/Cas9 screen identifies genes that regulate the cellular uptake of α-synuclein fibrils by modulating heparan sulfate proteoglycans. *bioRxiv* 2023**:** 2023.2009.2029.560170.

32. van den Born, J.; Salmivirta, K.; Henttinen, T.; Östman, N.; Ishimaru, T.; Miyaura, S.; Yoshida, K.; Salmivirta, M. Novel Heparan Sulfate Structures Revealed by Monoclonal Antibodies*. *Journal of Biological Chemistry* 2005, **280**(21)**:** 20516-20523.

33. Oakley, J. V.; Buksh, B. F.; Fernández, D. F.; Oblinsky, D. G.; Seath, C. P.; Geri, J. B.; Scholes, G. D.; MacMillan, D. W. C. Radius measurement via super-resolution microscopy enables the development of a variable radii proximity labeling platform. *Proceedings of the National Academy of Sciences* 2022, **119**(32)**:** e2203027119.

34. Huppertz, I.; Perez-Perri, J. I.; Mantas, P.; Sekaran, T.; Schwarzl, T.; Russo, F.; Ferring-Appel, D.; Koskova, Z.; Dimitrova-Paternoga, L.; Kafkia, E.; Hennig, J.; Neveu, P. A.; Patil, K.; Hentze, M. W. Riboregulation of Enolase 1 activity controls glycolysis and embryonic stem cell differentiation. *Molecular Cell* 2022, **82**(14)**:** 2666-2680.e2611.

35. Timchenko, L. T.; Iakova, P.; Welm, A. L.; Cai, Z. J.; Timchenko, N. A. Calreticulin Interacts with C/EBPα and C/EBPβ mRNAs and Represses Translation of C/EBP Proteins. *Molecular and Cellular Biology* 2002, **22**(20)**:** 7242-7257.

36. Caudron-Herger, M.; Jansen, R. E.; Wassmer, E.; Diederichs, S. RBP2GO: a comprehensive pan-species database on RNA-binding proteins, their interactions and functions. *Nucleic Acids Research* 2021, **49**(D1)**:** D425-D436.

37. Caudron-Herger, M.; Rusin, S. F.; Adamo, M. E.; Seiler, J.; Schmid, V. K.; Barreau, E.; Kettenbach, A. N.; Diederichs, S. R-DeeP: Proteome-wide and Quantitative Identification of RNA-Dependent Proteins by Density Gradient Ultracentrifugation. *Molecular Cell* 2019, **75**(1)**:** 184-199.e110.

38. Stanietsky, N.; Simic, H.; Arapovic, J.; Toporik, A.; Levy, O.; Novik, A.; Levine, Z.; Beiman, M.; Dassa, L.; Achdout, H.; Stern-Ginossar, N.; Tsukerman, P.; Jonjic, S.; Mandelboim, O.

The interaction of TIGIT with PVR and PVRL2 inhibits human NK cell cytotoxicity. *Proceedings of the National Academy of Sciences* 2009, **106**(42)**:** 17858-17863.

39. Fuchs, A.; Cella, M.; Giurisato, E.; Shaw, A. S.; Colonna, M. Cutting Edge: CD96 (Tactile) Promotes NK Cell-Target Cell Adhesion by Interacting with the Poliovirus Receptor (CD155). *The Journal of Immunology* 2004, **172**(7)**:** 3994-3998.

40. Wojtowicz, W. M.; Vielmetter, J.; Fernandes, R. A.; Siepe, D. H.; Eastman, C. L.; Chisholm, G. B.; Cox, S.; Klock, H.; Anderson, P. W.; Rue, S. M.; Miller, J. J.; Glaser, S. M.; Bragstad, M. L.; Vance, J.; Lam, A. W.; Lesley, S. A.; Zinn, K.; Garcia, K. C. A Human IgSF Cell-Surface Interactome Reveals a Complex Network of Protein-Protein Interactions. *Cell* 2020, **182**(4)**:** 1027-1043.e1017.

41. Pende, D.; Bottino, C.; Castriconi, R.; Cantoni, C.; Marcenaro, S.; Rivera, P.; Spaggiari, G. M.; Dondero, A.; Carnemolla, B.; Reymond, N.; Mingari, M. C.; Lopez, M.; Moretta, L.; Moretta, A. PVR (CD155) and Nectin-2 (CD112) as ligands of the human DNAM-1 (CD226) activating receptor: involvement in tumor cell lysis. *Molecular Immunology* 2005, **42**(4)**:** 463-469.

42. Lucas, R.; Gómez-Pinto, I.; Aviñó, A.; Reina, J. J.; Eritja, R.; González, C.; Morales, J. C. Highly Polar Carbohydrates Stack onto DNA Duplexes via CH/π Interactions. *Journal of the American Chemical Society* 2011, **133**(6)**:** 1909-1916.

43. Castello, A.; Fischer, B.; Frese, Christian K.; Horos, R.; Alleaume, A.-M.; Foehr, S.; Curk, T.; Krijgsveld, J.; Hentze, Matthias W. Comprehensive Identification of RNA-Binding Domains in Human Cells. *Molecular Cell* 2016, **63**(4)**:** 696-710.

44. Cardin, A. D.; Weintraub, H. J. Molecular modeling of protein-glycosaminoglycan interactions. *Arteriosclerosis* 1989, **9**(1)**:** 21-32.

45. del Carmen Fernandez-Alonso, M.; Diaz, D.; Alvaro Berbis, M.; Marcelo, F.; Canada, J.; Jimenez-Barbero, J. Protein-Carbohydrate Interactions Studied by NMR: From Molecular Recognition to Drug Design. *Current Protein & Peptide Science* 2012, **13**(8)**:** 816-830.

46. Schwarz, F. P.; Puri, K. D.; Bhat, R. G.; Surolia, A. Thermodynamics of monosaccharide binding to concanavalin A, pea (Pisum sativum) lectin, and lentil (Lens culinaris) lectin. *Journal of Biological Chemistry* 1993, **268**(11)**:** 7668-7677.

47. Kiessling, L. L.; Young, T.; Gruber, T. D.; Mortell, K. H. Multivalency in Protein–Carbohydrate Recognition. In: Fraser-Reid BO, Tatsuta K, Thiem J (eds). *Glycoscience: Chemistry and Chemical Biology*. Springer Berlin Heidelberg: Berlin, Heidelberg, 2008, pp 2483-2523.

48. Xue, S.; Zhou, F.; Zhao, T.; Zhao, H.; Wang, X.; Chen, L.; Li, J.-p.; Luo, S.-Z. Phase separation on cell surface facilitates bFGF signal transduction with heparan sulphate. *Nature Communications* 2022, **13**(1)**:** 1112.

49. Klein, K.; Hölzemer, A.; Wang, T.; Kim, T.-E.; Dugan, H. L.; Jost, S.; Altfeld, M.; Garcia-Beltran, W. F. A Genome-Wide CRISPR/Cas9-Based Screen Identifies Heparan Sulfate Proteoglycans as Ligands of Killer-Cell Immunoglobulin-Like Receptors. *Frontiers in Immunology* 2021, **12**.

50. Xu, D.; Young, J. H.; Krahn, J. M.; Song, D.; Corbett, K. D.; Chazin, W. J.; Pedersen, L. C.; Esko, J. D. Stable RAGE-Heparan Sulfate Complexes Are Essential for Signal Transduction. *ACS Chemical Biology* 2013, **8**(7)**:** 1611-1620.

51. Sirois, C. M.; Jin, T.; Miller, A. L.; Bertheloot, D.; Nakamura, H.; Horvath, G. L.; Mian, A.; Jiang, J.; Schrum, J.; Bossaller, L.; Pelka, K.; Garbi, N.; Brewah, Y.; Tian, J.; Chang, C.; Chowdhury, P. S.; Sims, G. P.; Kolbeck, R.; Coyle, A. J.; Humbles, A. A.; Xiao, T. S.; Latz, E. RAGE is a nucleic acid receptor that promotes inflammatory responses to DNA. *Journal of Experimental Medicine* 2013, **210**(11)**:** 2447-2463.

52. Termaat, R.-M.; Brinkman, K.; van Gompel, F.; van den Heuvel, L. P. W. J.; Veerkamp, J. H.; Smeenk, R. J. T.; Berden, J. H. M. Cross-reactivity of monoclonal anti-DNA antibodies with heparan sulfate is mediated via bound DNA/histone complexes. *Journal of Autoimmunity* 1990, **3**(5)**:** 531-545.

53. Park, H.; Kim, M.; Kim, H.-J.; Lee, Y.; Seo, Y.; Pham, C. D.; Lee, J.; Byun, S. J.; Kwon, M.-H. Heparan sulfate proteoglycans (HSPGs) and chondroitin sulfate proteoglycans (CSPGs) function as endocytic receptors for an internalizing anti-nucleic acid antibody. *Scientific Reports* 2017, **7**(1)**:** 14373.

54. Gruner, H. N.; McManus, M. T. Examining the evidence for extracellular RNA function in mammals. *Nature Reviews Genetics* 2021, **22**(7)**:** 448-458.

55. Ren, Z.; Li, R.; Zhou, X.; Chen, Y.; Fang, Y.; Zou, P. Enzyme-Mediated Proximity Labeling Identifies Small RNAs in the Endoplasmic Reticulum Lumen. *Biochemistry* 2023, **62**(12)**:** 1844-1848.

56. Zhang, M.; Liu, L.; Lin, X.; Wang, Y.; Li, Y.; Guo, Q.; Li, S.; Sun, Y.; Tao, X.; Zhang, D.; Lv, X.; Zheng, L.; Ge, L. A Translocation Pathway for Vesicle-Mediated Unconventional Protein Secretion. *Cell* 2020, **181**(3)**:** 637-652.e615.

57. Luteijn Rutger, D.; van Diemen, F.; Blomen Vincent, A.; Boer Ingrid, G. J.; Manikam Sadasivam, S.; van Kuppevelt Toin, H.; Drexler, I.; Brummelkamp Thijn, R.; Lebbink Robert, J.; Wiertz Emmanuel, J. A Genome-Wide Haploid Genetic Screen Identifies Heparan Sulfate-Associated Genes and the Macropinocytosis Modulator TMED10 as Factors Supporting Vaccinia Virus Infection. *Journal of Virology* 2019, **93**(13)**:** 10.1128/jvi.02160-02118.

58. Faas, F. G. A.; Avramut, M. C.; M. van den Berg, B.; Mommaas, A. M.; Koster, A. J.; Ravelli, R. B. G. Virtual nanoscopy: Generation of ultra-large high resolution electron microscopy maps. *Journal of Cell Biology* 2012, **198**(3)**:** 457-469.

59. Santos-Barriopedro, I.; van Mierlo, G.; Vermeulen, M. Off-the-shelf proximity biotinylation for interaction proteomics. *Nature Communications* 2021, **12**(1)**:** 5015.

60. Joung, J.; Konermann, S.; Gootenberg, J. S.; Abudayyeh, O. O.; Platt, R. J.; Brigham, M. D.; Sanjana, N. E.; Zhang, F. Genome-scale CRISPR-Cas9 knockout and transcriptional activation screening. *Nature Protocols* 2017, **12**(4)**:** 828-863.

61. Spahn, P. N.; Bath, T.; Weiss, R. J.; Kim, J.; Esko, J. D.; Lewis, N. E.; Harismendy, O. PinAPL-Py: A comprehensive web-application for the analysis of CRISPR/Cas9 screens. *Scientific Reports* 2017, **7**(1)**:** 15854.